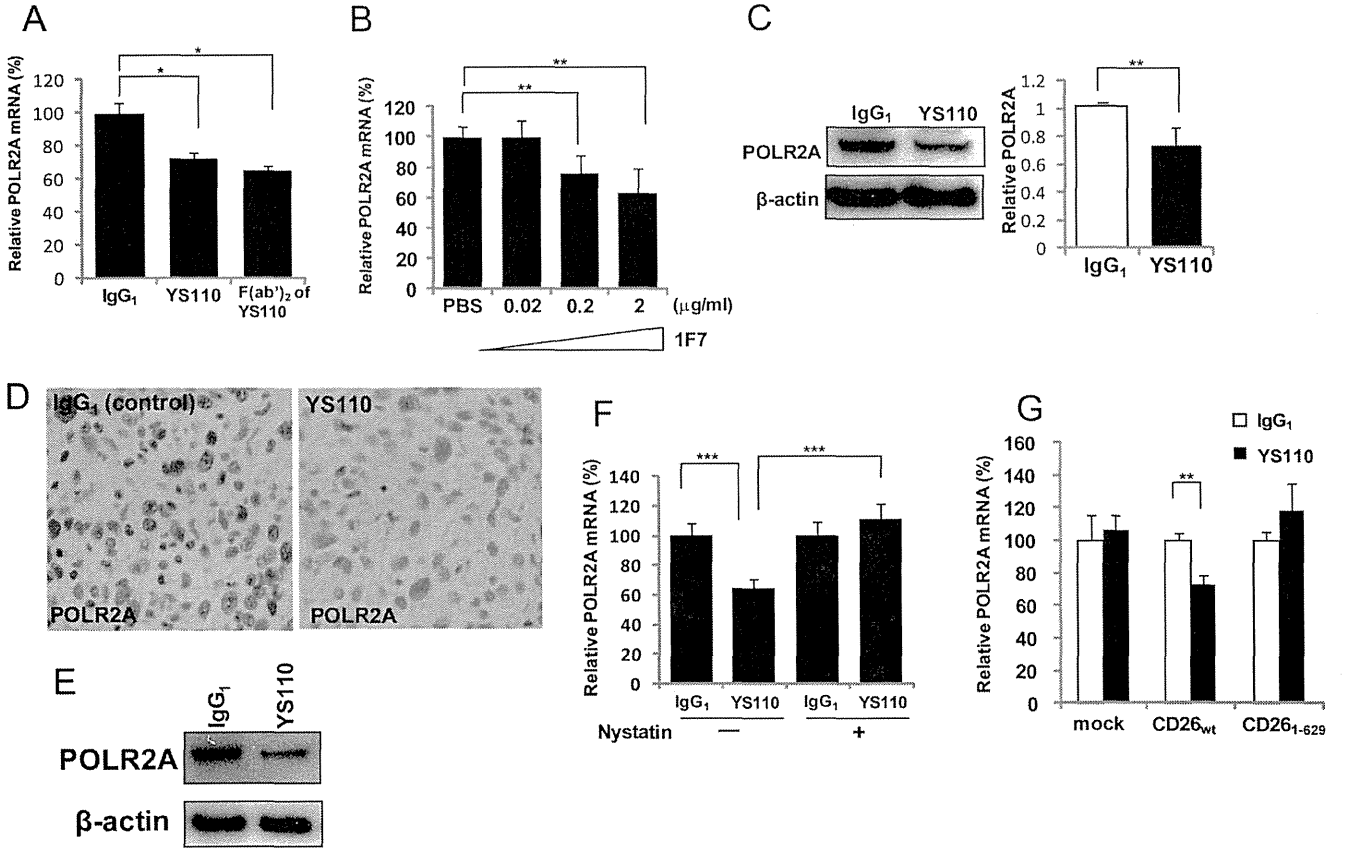

Figure 6. Nuclear Translocation of CD26 After Treatment with YS110 or 1F7 Suppresses POLR2A Expression. (A) Quantitative RT-PCR analysis of POLR2A mRNA in JMN cells treated with YS110 or YS110-F(ab')$_2$ (2 μg/mL) for 3 hours, relative to that in JMN cells treated with control human IgG$_1$. Data were normalized to glyceraldehyde-3-phosphate dehydrogenase (GAPDH) mRNA levels and are means ± SD from three independent experiments. *P<0.01. (B) Quantitative RT-PCR analysis of POLR2A mRNA in JMN cells treated with 1F7 (0.02, 0.2, or 2 μg/mL) for 3 hours, relative to that in JMN cells treated with IgG$_1$. Data were normalized to GAPDH mRNA levels and are means ± SD from three independent experiments. **P<0.025. (C) Upper panels show immunoblot analysis of POLR2A and β-actin (loading control) in lysates of JMN cells treated with control IgG$_1$ or YS110 (2 μg/mL) for 3 hours. Lower panel shows mean values (± SD) from three independent experiments, for intensity of the POLR2A band in cells treated with YS110, relative to that in cells treated with control IgG$_1$. (D) Immunostaining for POLR2A of tumors from NOG mice inoculated with JMN cells, followed by one intratumoral injection of control IgG$_1$ or YS110 (1 μg/a tumor, volume is 100 μL). Scale bars, 20 μm. (E) Immunoblot of POLR2A and β-actin (loading control) in lysates of tumors from NOG mice inoculated with JMN cells, followed by one intratumoral injection of control IgG$_1$ or YS110 (1 μg/a tumor, volume is 100 μL). (F) Quantitative RT-PCR analysis of *POLR2A* mRNA in JMN cells treated with human control IgG$_1$ or YS110 (2 μg/mL) for 3 hours, after pretreatment with DMSO or nystatin (50 μg/mL) for 30 minutes. Data were normalized to GAPDH mRNA levels and are means ± SD from three independent experiments. ***P<0.005. (G) Quantitative RT-PCR analysis of POLR2A mRNA in Li7 cells transfected with control, CD26$_{wt}$, or CD26$_{1-629}$ constructs, following treatment with human control IgG$_1$ or YS110 (2 μg/mL) for 3 hours. Data were normalized to GAPDH mRNA levels and are means ± SD from three independent experiments. **P<0.025.
doi:10.1371/journal.pone.0062304.g006

Discussion

Various cancer-related cell-surface proteins are known to be transported into the nucleus in several cancers, including ErbB2 (breast cancer), CD40 (lymphoma), and CD44 (breast cancer) [18,19,37]. The nuclear function of these receptors is implicated in critical cellular processes, from signal transduction to cell proliferation, which underscores the importance of the nuclear function of membrane receptors in cancer treatment [38]. In this study, we examined the significance of the nuclear localization of CD26 in its role as a mAb therapy for CD26-positive cancers, and showed that nuclear translocation of CD26 induced by YS110 treatment reduces cell growth through transcriptional repression of the POLR2A gene. Furthermore, we found that YS110 is itself translocated to the nucleus by a mechanism that depends on the C-terminus of CD26 (Fig. 2E; Fig. S3B). These studies highlight the function of CD26 that is translocated to the nucleus in cell growth regulation, and indicate an important mechanism by which mAb therapy targets the cell-surface antigen, CD26, that is able to translocate to the nucleus.

CD26 expression has been shown to be associated with tumor formation and metastasis [5]. We previously reported that cytoplasmic, but not cell surface, expression of CD26 in patients with malignant mesothelioma was correlated with a poor prognosis and chemo-resistance [7,8]. These previous observations, together with the present findings, suggest that CD26 contributes to both tumor development and tumor growth retardation. It is possible that these reciprocal functions of CD26 in cancer cells may be determined by its functional subcellular localization, through the action of different stimuli. Therefore, we speculate that nuclear CD26 may serve as a "brake" on tumor growth. In keeping with this, other studies have shown that nuclear ErbB-2 is involved in the progression of breast carcinoma [39]. Furthermore, EGFR is known to undergo nuclear localization in regenerating hepatocytes [40].

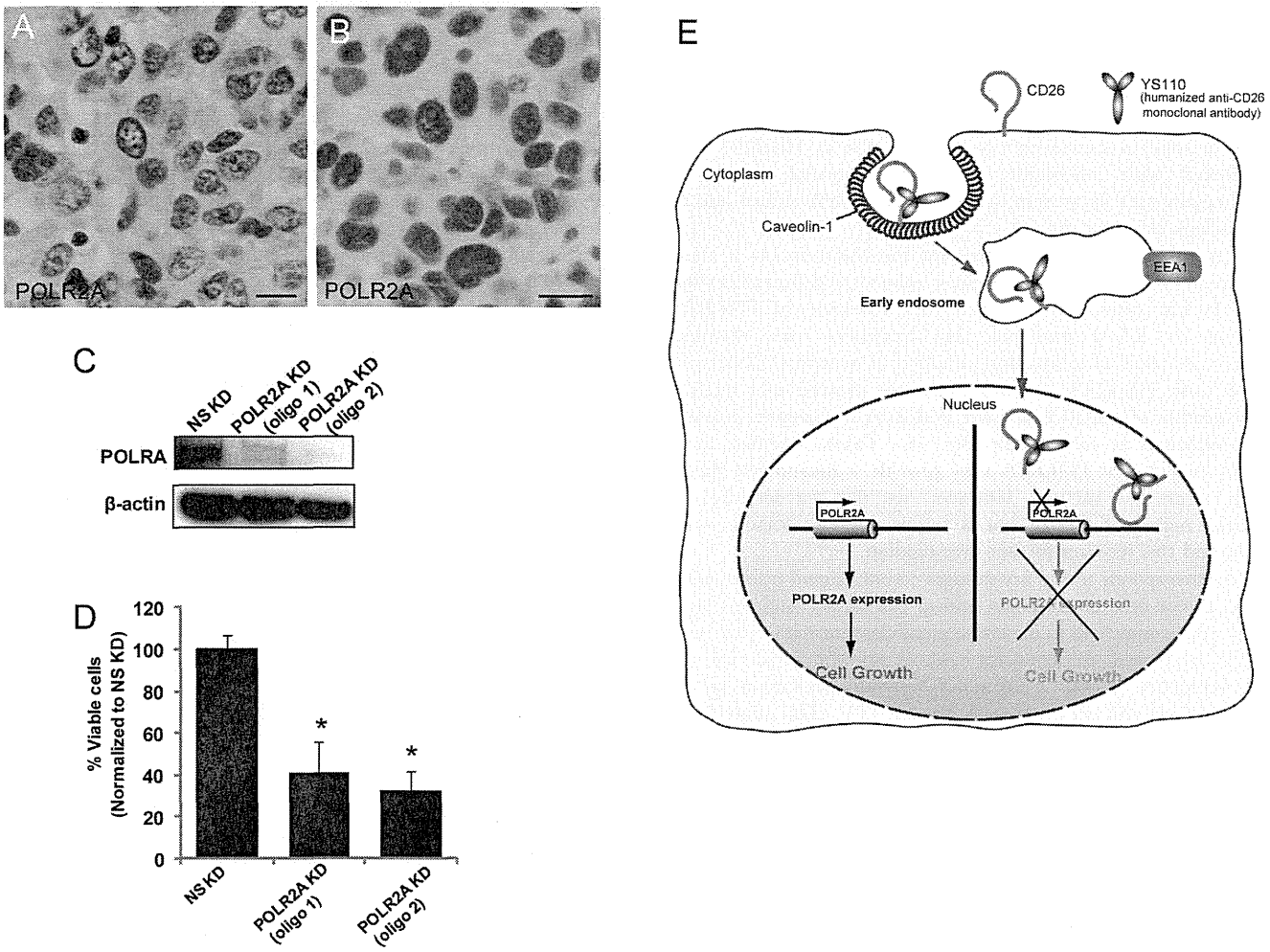

Figure 7. Knock-Down of the POLR2A Gene Inhibits Cell Growth in JMN Cells. (A) Immunostaining of POLR2A in tumors from malignant mesothelioma patients. Scale bar, 20 μm. (B) Immunostaining of POLR2A in tumors from NOG mice inoculated with MSTO/CD26 cells. Scale bar, 20 μm. (C) Immunoblot analysis of POLR2A in JMN cells transfected with a non-specific (NS) control siRNA or POLR2A siRNA (oligo 1 or oligo 2). β-actin was used as a loading control. KD, knock-down. (D) Numbers of viable JMN cells transfected with POLR2A siRNA (oligo 1 or oligo 2) for 48 hours, relative into the numbers of viable cells transfected with NS control siRNA, were measured using the water soluble, 2-(2-methoxy-4-nitrophenyl)-3-(4-nitrophenyl)-5-(2,4-disulfophenyl)-2H-tetrazolium (WST)-8 assay. Data are means ± SD from three independent experiments. *$P<0.004$. (E) Model for POLR2A suppression by YS110-induced nuclear CD26. Cell surface CD26 is translocated to the nucleus in response to YS110 treatment, and binds to genomic DNA associated with the POLR2A gene. This results in transcriptional suppression of POLR2A and consequent inhibition of cell growth.
doi:10.1371/journal.pone.0062304.g007

Taken together, the nuclear translocation and the nuclear function of transmembrane proteins provide important insights into understanding the intricate cellular processes involved in development, differentiation, and tumorigenesis, and may lead to the identification of therapeutic targets for specific antigen-responsive disorders, including cancers.

The nuclear entry of most membrane proteins is thought to be mediated by mechanisms involving endocytosis and early endosomal sorting [18]. EEA1, an early endocytic protein, is known to interact with other receptors that are translocated into the nucleus, including EGFR and ErbB-2 [34,35]. The present study showed that YS110 colocalized with EEA1, both in the cytoplasm and in the nucleus, and that transfection with a dominant-negative mutant of Rab5A, a master regulator of endosome biogenesis, prevented the nuclear translocation of YS110 (Fig. S5E). These findings suggest that early endocytic vesicles may function as carriers of cargo proteins toward the nucleus.

Furthermore, impairment of caveolin-dependent endocytosis inhibited the nuclear entry of both CD26 and YS110, and subsequent suppression of POLR2A, suggesting that the caveolin-dependent endocytic pathway is required for nuclear translocation of CD26 and YS110. Given that CD26 contains no putative nuclear localization signal (NLS) sequence, and that nuclear trafficking of CD26 and YS110 relies on the C-terminal extracellular domain of CD26 (Fig. 2E; Fig. S3B), we assume the presence of putative partners interacting with CD26. The partners presumably contain well-known nuclear accessible domains, such as NLS, and bind to CD26 through its C-terminus domain, either at the raft-domain or during endosomal trafficking associated with the early endosome. The formation of such a complex would allow full-length CD26 to pass through the nuclear membrane into the nucleus. When this interaction between the putative partners and CD26 is disrupted, the import of CD26 from the cytoplasm into the nucleus is impaired, resulting in a loss of function of nuclear CD26. Therefore, spatial expression of the

putative partners may be an indispensable and rate-limiting step in both the nuclear transport and function of CD26, and this may provide one explanation for the small amount of nuclear CD26, even after YS110 treatment. In support of this, the present data showed that YS110-induced nuclear induction of CD26 did not occur in some non-neoplastic cell lines, such as HEK293 cells transfected with full-length CD26, and normal human T lymphocytes with expression of CD26 on the cell surface and in the nucleus (data not shown).

RNA polymerase II is essential for the transcription of most protein-coding genes, including those related to cell proliferation [23]. It was previously reported that blockade of POLR2A function by RNAi strategies, and treatment with chemical compounds such as α-amanitin, resulted in growth inhibition of cancer cells [41,42,43]. In this study, we showed that nuclear accumulation of CD26 promoted POLR2A suppression, leading to a reduction in cell growth (Fig. 7E). Taken together, these results suggest that POLR2A may provide a meaningful therapeutic target for cancers. However, we did not identify the essential region of CD26 that is required for association with DNA, and this requires further investigation.

Most therapeutic mAbs are thought to alter signal transduction within tumor cells or eliminate critical cell-surface antigens [11]. These effects may lead to the consequent clearance of cancer cells. ErbB2 is known to associate with a specific locus on the cyclooxygenase (COX) 2 promoter, activate expression of the gene, and thereby promote cell growth [39]. The humanized ErbB2 mAb trastuzumab (Herceptin) impairs the translocation of ErbB2 into the nucleus. The present study revealed that in contrast to this ErbB2-Herceptin axis, YS110 treatment abundantly augments nuclear localization of CD26, and consequently suppresses POLR2A expression, leading to inhibition of malignant mesothelioma cell growth. These findings suggest that alteration of nuclear transport of cell-surface antigens by mAbs may represent an effective target for mAb therapy of cancers.

Almost all patients with malignant mesothelioma cases have positive CD26 [7]. In this study, we showed the nuclear localization of CD26 in the samples taken from malignant mesothelioma patients. However, whether the extent of the nuclear localization is dependent on cancer types, tumor stages, and milieu or not needs further investigation. Currently, phase 1 clinical trial of YS100 treatment is conducting for malignant mesothelioma and renal cell carcinoma patients in France. The mechanism of anti-tumor machinery for YS100 and the current chemotherapeutic agents is different. Thus, combination between YS110 and standard therapy may have synergistic effects and enhance the treatment against malignant mesothelioma.

Recent studies have shown that various mAbs conjugated to payloads (e.g., radioisotopes, drugs, or toxins) may be targeted to directly kill tumor cells [44,45,46,47]. In fact, the 90Y-radiolabeled murine anti-CD20 IgG_1, Ibritumomab tiuxetan (Zevalin), has been proven to have substantial antitumor activity, and is used in standard clinical practice, as a therapy for lymphoma [48]. However, the potentially potent cytotoxicity of these payloads may impede the development of new conjugated antibodies. In this study, we demonstrated nuclear localization of anti-CD26 mAbs (YS110 and 1F7) in a cell-surface CD26-dependent manner. This implies that YS110 and 1F7 may target specific intra-nuclear components, such as genomic DNA and transcription factors. In addition to these antibodies, there have been previous reports on the nuclear localization of mAbs directed against cell-surface antigens, including ME425 (against EGF receptor) and Br 15-6A (carbohydrate Y determinant) [49,50]. Therefore, these observations provide an insight into the development of bispecific mAbs that more potently and effectively target nuclear components related to cancer growth and invasion.

In conclusion, the present data provides evidence that induced nuclear localization of CD26 by the humanized anti-CD26 mAb, YS110, promotes transcriptional repression of the POLR2A gene, resulting in growth suppression of cancer cells. Given that YS110 has a direct anti-proliferative effect on cancer cells, including malignant mesothelioma cells, these findings highlight the potential of rational therapy against CD26-positive cancers, not only through immunological ADCC and complementary activation effects, but also by direct inhibition of cancer cell growth.

Supporting Information

Figure S1 Inhibition of Cell Growth by YS110 Treatment in Cultured Cancer Cells. (A) JMN or MSTO cells were cultured overnight at a density of 2.5×10^3 cells/well in 96-well plates. Proliferation was measured 48 hours after treatment with YS110 at the indicated concentrations, in triplicate for each condition, using cell counting reagent, as described in the MATERIALS AND METHODS. The ratio of growth inhibition was calculated as the percentage reduction in absorbance of cells treated with YS110, relative to that in cells not treated with YS110. Data are means ± SD from three independent experiments. * $P<0.025$. (B) T cell lymphoma Karpas299 cells were cultured overnight at a density of 1×10^4 cells/well in 96-well plates. Proliferation was measured 24 hours after treatment with murine control mouse IgG_1 or 1F7 (2 μg/mL), in triplicate for each condition, using cell counting reagent, as described in the MATERIALS AND METHODS. The cell viability ratio was calculated as the percentage absorbance of cells treated with 1F7 relative to that of cells treated with IgG_1. Data are means ± SD from three independent experiments. * $P<0.025$.
(TIF)

Figure S2 Nuclear Localization of Various CD26 Constructs in Several Cancer Cell Lines. (A) Jurkat/CD26 cells treated with mouse control IgG_1 or 1F7 (2 μg/mL) for 1 hour were fractionated into membrane, cytoplasmic, and nuclear fractions, as described in the MATERIALS AND METHODS. Each fraction was subjected to immunoblot analysis with antibody to CD26. Nuc, nuclear fraction. Mem, membrane fraction. (B) Hepatocellular carcinoma Li7 cells transiently expressing each flag-tagged construct were treated with control IgG_1 or YS110 (2 μg/mL) for 3 hours, then subjected to subcellular fractionation, followed by immunoblot analysis with antibodies to Flag, Na^+/K^+ ATPase (as a cytosolic marker), and lamin A/C (as a nuclear marker). Nuc, nuclear fraction. Mem, membrane fraction.
(TIF)

Figure S3 Nuclear Observation of Various CD26 Constructs in Several Cancer Cell Lines. (A) Confocal visualization of GFP-$CD26_{wt}$, GFP-$CD26_{7-766}$, and GFP-$CD26_{1-629}$ in HEK 293 cells, treated or not treated with Alexa-YS110 for 5 minutes. Co-localization of GFP-$CD26_{1-629}$ with YS110 (red) appears as yellow. Scale bars, 10 μm. (B) Confocal visualization of GFP-$CD26_{wt}$ and GFP-$CD26_{1-629}$ in JMN cells incubated with or without Alexa-YS110 (2 μg/mL) for 30 minutes before fixation. Each GFP is shown in green, YS110 is shown in red, and the nucleus is shown in blue (Hoechst 33342). Co-localization of GFP-$CD26_{wt}$ and YS110 in the nucleus appears as white in the boxed region. Scale bars, 10 μm.
(TIF)

Figure S4 Nuclear Transport of CD26 Constructs Preferentially Expressed at the Cell-Surface in Jurkat/

CD26 Cells. (A) Cell surface proteins on Jurkat/CD26 cells were biotinylated using NHS-biotin, treated with control IgG_1 or 1F7 (2 μg/mL) for the indicated times, and then fractionated into three cellular fractions. Extracts of each fraction were immunoprecipitated with antibody to CD26, and subjected to immunoblot analysis using streptavidin. The relative intensities of the streptavidin bands in the nuclear (left panels) and membrane (right panels) fractions were assessed by densitometry. Data are means ± SD from three independent experiments. Nuc, nuclear fraction. Mem, membrane fraction. (B) Cell surface-biotinylated Jurkat/CD26 cells were treated with control IgG_1, 1F7, or 5F8 (2 μg/mL) for 1 hour before subcellular fractionation. Extracts of the membrane and nuclear fractions were immunoprecipitated with CD26 and subjected to immunoblot analysis with streptavidin. A representative immunoblot and the corresponding quantification are shown.
(TIF)

Figure S5 Involvement of the Caveolin-Dependent Endocytic Pathway in the Nuclear Localization of YS110. (A) JMN cells were treated with both Alexa-YS110 and Alexa-CtxB (2 μg/mL) for 10 or 30 minutes, fixed, and then stained with Hoechst 33342. The interaction of Alexa-YS110 and Alexa-CtxB (boxed regions) is demonstrated at higher magnification in the medium size images. Scale bars, 10 μm. (B) JMN cells were pretreated with chlorpromazine, an inhibitor for clathrin pathway, (10 μg/mL) for 30 minutes prior to treatment with Alexa-YS110 for 30 min. Endocytosis and nuclear localization of Alexa-YS110 (arrows) were observed by confocal fluorescence microscopy. (C) Immunofluorescence staining for YS110 (red), early endosome antigen (EEA) 1 (green), and Hoechst 33342 (blue) in fixed JMN cells, following treatment with Alexa-YS110 for 10 or 30 minutes. The boxed region in the panel shows co-localization of Alexa-YS110 with EEA1 in the nucleus (white) at high magnification. Scale bars, 10 μm. (D) Immunoelectron microscopic examination showed co-localization of EEA1 and YS110 in the nucleus of JMN cells. The arrow and arrowhead indicate EEA1 (15 nm) and YS110 (30 nm), respectively. Scale bar, 200 nm. Cy, cytoplasm; Nu, nucleus. (E) JMN cells were transfected with GFP-$Rab5A^{wt}$ or GFP-$Rab5A^{S34N}$. Each transfectant was treated with Alexa-YS110 for 30 minutes, fixed, then stained with Hoechst 33342. Localization of Alexa-YS110 (red) in the nucleus (blue) is indicated by arrows. Scale bars, 10 μm.
(TIF)

Figure S6 Inhibition of Tumor Growth by YS110 Treatment in a Malignant Mesothelioma Xenograft Model. Macroscopic images of tumors on chest walls that were developed in NOG mice orthotopically inoculated with MSTO/CD26 cells, after injection of control IgG_1, or YS110 (left image) in thoraxes. Right panels indicate the tumor weights of left thoraxes and pericardiums in mice orthotopically inoculated with MSTO/wt or MSTO/clone12 cells, after injection of control IgG_1 or YS110 in right thoraxes.
(TIF)

Figure S7 YS110 is Translocated to the Nucleus in Malignant Mesothelioma Tumors. Fluorescence analysis of subcutaneous JMN tumors from NOG mice, 1 hour after one intratumoral injection (1 μg/a tumor, volume is 100 μL) of Alexa647-human IgG_1 (A–C) or Alexa647-YS110 (D–F). In each image, Alexa647-labeled antibodies is shown in green (B, C, E and F), and the nucleus is shown in red (Hoechst 33342) (A, C, D and F). Localization of Alexa-YS110 in the nucleus is shown as yellow (arrows) (F). Similar results were obtained with three different mice. Scale bars, 10 μm.
(TIF)

Figure S8 ChIP Assay Using Different Primers for CAS162 in JMN cells and Reporter Assays in Various Cancer Cell Lines. (A) The interaction between CD26 and CAS162 was detected by ChIP assay using two different types of primers flanking CAS162. Results obtained using primer set #1 are shown in Figure 5C. (B) Hepatocellular carcinoma cell lines (Li7 without CD26 expression and Kim1 with CD26 expression) was co-transfected with pGL3 promoter vector (pGL3pro, as control) or pGL3 promoter-CAS162 vector (CAS162) and phRL-TK vector, and relative luciferase activity was measured using a luminometer. Data were normalized for luciferase activity in cells transfected with phRL-TK.
(TIF)

Figure S9 Quantitative RT-PCR Analysis of POLR2A in JMN and MSTO/CD26 Cells Treated with YS110, and Nuclear Localization of YS110-F(ab')$_2$. (A) Quantitative RT-PCR analysis of POLR2A mRNA in JMN cells treated with YS110 (2 μg/mL), at the indicated times (1, 3, 6, 12 and 24 hours), relative to the 0 hour control. Data were normalized to the expression of glyceraldehyde-3-phosphate dehydrogenase (GAPDH) mRNA and are means ± SD from three independent experiments. *$P<0.025$. **$P<0.006$. (B) Quantitative RT-PCR analysis of POLR2A mRNA in MSTO/CD26 cells treated with control IgG_1 or YS110 (2 μg/mL) for 3 hours. Data were normalized to the expression of GAPDH mRNA and are means ± SD from three independent experiments. *$P<0.025$.
(TIF)

Figure S10 Nuclear Localization of YS110-F(ab')$_2$. Immunoblot detection of YS110-F(ab')$_2$ in cytoplasmic and nuclear fractions of JMN or Alex (hepatocellular carcinoma) cells treated with YS110-F(ab')$_2$ (2 μg/mL) for 1 hour.
(TIF)

Acknowledgments

We thank Dr. T. Oikawa for providing the GFP-Rab5A constructs. We thank H. Abe and A. Sato for technical assistance.

Author Contributions

Conceived and designed the experiments: KY HM TY. Performed the experiments: KY MH HM. Analyzed the data: KY HM KO TY. Contributed reagents/materials/analysis tools: HN WD KO MS CM. Wrote the paper: KY KO TY.

References

1. Rasmussen HB, Branner S, Wiberg FC, Wagtmann N (2003) Crystal structure of human dipeptidyl peptidase IV/CD26 in complex with a substrate analog. Nat Struct Biol 10: 19–25.
2. Drucker DJ, Nauck MA (2006) The incretin system: glucagon-like peptide-1 receptor agonists and dipeptidyl peptidase-4 inhibitors in type 2 diabetes. Lancet 368: 1696–1705.
3. Havre PA, Abe M, Urasaki Y, Ohnuma K, Morimoto C, et al. (2008) The role of CD26/dipeptidyl peptidase IV in cancer. Front Biosci 13: 1634–1645.
4. Inamoto T, Yamada T, Ohnuma K, Kina S, Takahashi N, et al. (2007) Humanized anti-CD26 monoclonal antibody as a treatment for malignant mesothelioma tumors. Clin Cancer Res 13: 4191–4200.
5. Pang R, Law WL, Chu AC, Poon JT, Lam CS, et al. (2010) A subpopulation of CD26+ cancer stem cells with metastatic capacity in human colorectal cancer. Cell Stem Cell 6: 603–615.
6. Ghani FI, Yamazaki H, Iwata S, Okamoto T, Aoe K, et al. (2011) Identification of cancer stem cell markers in human malignant mesothelioma cells. Biochem Biophys Res Commun 404: 735–742.

7. Amatya VJ, Takeshima Y, Kushitani K, Yamada T, Morimoto C, et al. (2011) Overexpression of CD26/DPPIV in mesothelioma tissue and mesothelioma cell lines. Oncol Rep 26: 1369–1375.
8. Aoe K, Amatya VJ, Fujimoto N, Ohnuma K, Hosono O, et al. (2012) CD26 Overexpression Is Associated with Prolonged Survival and Enhanced Chemosensitivity in Malignant Pleural Mesothelioma. Clin Cancer Res 18: 1447–1456.
9. Inamoto T, Yamochi T, Ohnuma K, Iwata S, Kina S, et al. (2006) Anti-CD26 monoclonal antibody-mediated G1-S arrest of human renal clear cell carcinoma Caki-2 is associated with retinoblastoma substrate dephosphorylation, cyclin-dependent kinase 2 reduction, p27(kip1) enhancement, and disruption of binding to the extracellular matrix. Clin Cancer Res 12: 3470–3477.
10. Ho L, Aytac U, Stephens LC, Ohnuma K, Mills GB, et al. (2001) In vitro and in vivo antitumor effect of the anti-CD26 monoclonal antibody 1F7 on human CD30+ anaplastic large cell T-cell lymphoma Karpas 299. Clin Cancer Res 7: 2031–2040.
11. Adams GP, Weiner LM (2005) Monoclonal antibody therapy of cancer. Nat Biotechnol 23: 1147–1157.
12. Steplewski Z, Lubeck MD, Koprowski H (1983) Human macrophages armed with murine immunoglobulin G2a antibodies to tumors destroy human cancer cells. Science 221: 865–867.
13. Sliwkowski MX, Lofgren JA, Lewis GD, Hotaling TE, Fendly BM, et al. (1999) Nonclinical studies addressing the mechanism of action of trastuzumab (Herceptin). Semin Oncol 26: 60–70.
14. Weng WK, Levy R (2003) Two immunoglobulin G fragment C receptor polymorphisms independently predict response to rituximab in patients with follicular lymphoma. J Clin Oncol 21: 3940–3947.
15. Benmerah A (2004) Endocytosis: signaling from endocytic membranes to the nucleus. Curr Biol 14: R314–316.
16. Miaczynska M, Bar-Sagi D (2010) Signaling endosomes: seeing is believing. Curr Opin Cell Biol 22: 535–540.
17. Stachowiak EK, Maher PA, Tucholski J, Mordechai E, Joy A, et al. (1997) Nuclear accumulation of fibroblast growth factor receptors in human glial cells–association with cell proliferation. Oncogene 14: 2201–2211.
18. Wang YN, Yamaguchi H, Hsu JM, Hung MC (2010) Nuclear trafficking of the epidermal growth factor receptor family membrane proteins. Oncogene 29: 3997–4006.
19. Lin-Lee YC, Pham LV, Tamayo AT, Fu L, Zhou HJ, et al. (2006) Nuclear localization in the biology of the CD40 receptor in normal and neoplastic human B lymphocytes. J Biol Chem 281: 18878–18887.
20. Yamada K, Hayashi M, Du W, Ohnuma K, Sakamoto M, et al. (2009) Localization of CD26/DPPIV in nucleus and its nuclear translocation enhanced by anti-CD26 monoclonal antibody with anti-tumor effect. Cancer Cell Int 9: 17.
21. Kotani T, Kawano J, Suganuma T, Hirai K, Umeki K, et al. (1992) Immunohistochemical localization of dipeptidyl aminopeptidase IV in thyroid papillary carcinoma. Int J Exp Pathol 73: 215–222.
22. Ohnuma K, Ishii T, Iwata S, Hosono O, Kawasaki H, et al. (2002) G1/S cell cycle arrest provoked in human T cells by antibody to CD26. Immunology 107: 325–333.
23. Wintzerith M, Acker J, Vicaire S, Vigneron M, Kedinger C (1992) Complete sequence of the human RNA polymerase II largest subunit. Nucleic Acids Res 20: 910.
24. Kittler JT, Thomas P, Tretter V, Bogdanov YD, Haucke V, et al. (2004) Huntingtin-associated protein 1 regulates inhibitory synaptic transmission by modulating gamma-aminobutyric acid type A receptor membrane trafficking. Proc Natl Acad Sci U S A 101: 12736–12741.
25. Fairfax BP, Pitcher JA, Scott MG, Calver AR, Pangalos MN, et al. (2004) Phosphorylation and chronic agonist treatment atypically modulate GABAB receptor cell surface stability. J Biol Chem 279: 12565–12573.
26. Nojima T, Hirose T, Kimura H, Hagiwara M (2007) The interaction between cap-binding complex and RNA export factor is required for intronless mRNA export. J Biol Chem 282: 15645–15651.
27. Kounnis V, Ioachim E, Svoboda M, Tzakos A, Sainis I, et al. (2011) Expression of organic anion-transporting polypeptides 1B3, 1B1, and 1A2 in human pancreatic cancer reveals a new class of potential therapeutic targets. Onco Targets Ther 4: 27–32.
28. Yamamoto H, Komekado H, Kikuchi A (2006) Caveolin is necessary for Wnt-3a-dependent internalization of LRP6 and accumulation of beta-catenin. Dev Cell 11: 213–223.
29. McMahon HT, Boucrot E (2011) Molecular mechanism and physiological functions of clathrin-mediated endocytosis. Nat Rev Mol Cell Biol 12: 517–533.
30. Duchardt F, Fotin-Mleczek M, Schwarz H, Fischer R, Brock R (2007) A comprehensive model for the cellular uptake of cationic cell-penetrating peptides. Traffic 8: 848–866.
31. Ohnuma K, Uchiyama M, Yamochi T, Nishibashi K, Hosono O, et al. (2007) Caveolin-1 triggers T-cell activation via CD26 in association with CARMA1. J Biol Chem 282: 10117–10131.
32. Sonnichsen B, De Renzis S, Nielsen E, Rietdorf J, Zerial M (2000) Distinct membrane domains on endosomes in the recycling pathway visualized by multicolor imaging of Rab4, Rab5, and Rab11. J Cell Biol 149: 901–914.
33. Zerial M, McBride H (2001) Rab proteins as membrane organizers. Nat Rev Mol Cell Biol 2: 107–117.
34. Giri DK, Ali-Seyed M, Li LY, Lee DF, Ling P, et al. (2005) Endosomal transport of ErbB-2: mechanism for nuclear entry of the cell surface receptor. Mol Cell Biol 25: 11005–11018.
35. Lo HW, Ali-Seyed M, Wu Y, Bartholomeusz G, Hsu SC, et al. (2006) Nuclear-cytoplasmic transport of EGFR involves receptor endocytosis, importin beta1 and CRM1. J Cell Biochem 98: 1570–1583.
36. Calera MR, Zamora-Ramos C, Araiza-Villanueva MG, Moreno-Aguilar CA, Pena-Gomez SG, et al. (2011) Parcs/Gpn3 is required for the nuclear accumulation of RNA polymerase II. Biochim Biophys Acta 1813: 1708–1716.
37. Okamoto I, Kawano Y, Murakami D, Sasayama T, Araki N, et al. (2001) Proteolytic release of CD44 intracellular domain and its role in the CD44 signaling pathway. J Cell Biol 155: 755–762.
38. Wang SC, Hung MC (2009) Nuclear translocation of the epidermal growth factor receptor family membrane tyrosine kinase receptors. Clin Cancer Res 15: 6484–6489.
39. Wang SC, Lien HC, Xia W, Chen IF, Lo HW, et al. (2004) Binding at and transactivation of the COX-2 promoter by nuclear tyrosine kinase receptor ErbB-2. Cancer Cell 6: 251–261.
40. Marti U, Burwen SJ, Wells A, Barker ME, Huling S, et al. (1991) Localization of epidermal growth factor receptor in hepatocyte nuclei. Hepatology 13: 15–20.
41. Mook OR, Baas F, de Wissel MB, Fluiter K (2009) Allele-specific cancer cell killing in vitro and in vivo targeting a single-nucleotide polymorphism in POLR2A. Cancer Gene Ther 16: 532–538.
42. Sudo H, Tsuji AB, Sugyo A, Kohda M, Sogawa C, et al. (2010) Knockdown of COPA, identified by loss-of-function screen, induces apoptosis and suppresses tumor growth in mesothelioma mouse model. Genomics 95: 210–216.
43. Arima Y, Nitta M, Kuninaka S, Zhang D, Fujiwara T, et al. (2005) Transcriptional blockade induces p53-dependent apoptosis associated with translocation of p53 to mitochondria. J Biol Chem 280: 19166–19176.
44. Francis RJ, Sharma SK, Springer C, Green AJ, Hope-Stone LD, et al. (2002) A phase I trial of antibody directed enzyme prodrug therapy (ADEPT) in patients with advanced colorectal carcinoma or other CEA producing tumours. Br J Cancer 87: 600–607.
45. Kreitman RJ, Wilson WH, Bergeron K, Raggio M, Stetler-Stevenson M, et al. (2001) Efficacy of the anti-CD22 recombinant immunotoxin BL22 in chemotherapy-resistant hairy-cell leukemia. N Engl J Med 345: 241–247.
46. Sievers EL, Appelbaum FR, Spielberger RT, Forman SJ, Flowers D, et al. (1999) Selective ablation of acute myeloid leukemia using antibody-targeted chemotherapy: a phase I study of an anti-CD33 calicheamicin immunoconjugate. Blood 93: 3678–3684.
47. Weiner LM, Murray JC, Shuptrine CW (2012) Antibody-based immunotherapy of cancer. Cell 148: 1081–1084.
48. Gordon LI, Witzig T, Molina A, Czuczman M, Emmanouilides C, et al. (2004) Yttrium 90-labeled ibritumomab tiuxetan radioimmunotherapy produces high response rates and durable remissions in patients with previously treated B-cell lymphoma. Clin Lymphoma 5: 98–101.
49. Rakowicz-Szulczynska EM, Koprowski H (1989) Nuclear uptake of monoclonal antibody to a surface glycoprotein and its effect on transcription. Arch Biochem Biophys 271: 366–379.
50. Rakowicz-Szulczynska EM, Steplewski Z, Koprowski H (1992) Nuclear translocation of monoclonal antibody directed against cell-surface carbohydrate Y determinant. Am J Pathol 141: 937–947.

Biochemical and Biophysical Research Communications 436 (2013) 121–127

Contents lists available at SciVerse ScienceDirect

Biochemical and Biophysical Research Communications

journal homepage: www.elsevier.com/locate/ybbrc

Multiple effects of repetitive transcranial magnetic stimulation on neuropsychiatric disorders

Tetsurou Ikeda [a,c,*], Masaru Kurosawa [a], Chikao Morimoto [c], Shigeo Kitayama [b], Nobuyuki Nukina [a]

[a] Laboratory for Structural Neuropathology, RIKEN Brain Science Institute, 2-1 Hirosawa, Wako-shi, Saitama 351-0198, Japan
[b] Department of Dental Pharmacology, Okayama University, Graduate School of Medicine and Dentistry, Shikata 2-5-1, Okayama 700-8525, Japan
[c] Clinical Immunology, Institute of Medical Science, The University of Tokyo, 4-6-1 Shirokanedai, Minato-ku, Tokyo 108-8639, Japan

ARTICLE INFO

Article history:
Received 22 February 2013
Available online 21 March 2013

Keywords:
rTMS
Period 2
HSP70
Dopamine receptor 2

ABSTRACT

Repetitive transcranial magnetic stimulation (rTMS) is a new tool that has been used for the treatment of patients with neuropsychiatric disorders. However, the mechanisms underlying the effects of rTMS are still unclear. We analyzed the changes in mRNA expression in mouse brain that occurred after rTMS with an Affymetrix GeneChip. Following 20 days of rTMS, many genes were differentially expressed in the mouse brain. Downregulation of Period 2 and 3 mRNA expression levels and a subsequent decrease in food and water intake were observed. HSP70 mRNA expression levels were upregulated after transient and chronic rTMS. In N2A 150Q cells, an upregulation of HSP70 mRNA and protein levels and subsequent cell-protective effects were observed after chronic rTMS. In addition, dopamine receptor 2 mRNA expression levels were downregulated, and a subsequent decrease in the binding of [^{3}H]raclopride was observed. These results indicated that the modulation of several genes may be involved in the therapeutic mechanisms of chronic rTMS for patients with neuropsychiatric disorders.

1. Introduction

Repetitive transcranial magnetic stimulation (rTMS) is a novel tool that is considered to induce electric currents in the brain through a coil [1–4]. Initially, Merton and Morton [5] showed that it is possible to stimulate the motor areas of the human brain electrically through the intact scalp (transcranial electrical stimulation). Barker and his group later showed that it was possible to stimulate both nerves and the brain with external magnetic stimulation [1], which is a technique known as TMS. Recently, TMS has been used as a diagnostic tool in neurology for measuring central motor conduction because it is painless and noninvasive [6]. In contrast, electroconvulsive therapy provides highly reliable relief from depressive symptoms, but intense electrical stimulation is required because the skull resists electric currents [7]. The intensity of the stimulation that is usually used to treat patients induces a sustained after-discharge in cortical neurons, which causes convulsive seizures. After TMS was introduced, it was shown to have several therapeutic benefits in patients with neuropsychiatric disorders, such as depression, Parkinson's disease, and schizophrenia [8–10]. These neuropsychiatric disorders are considered to be associated with monoamine systems. Because of its safety and relative painlessness, TMS has many possible applications as a therapeutic device, and it may be beneficial in the treatment of some psychiatric disorders that have not yet been explored. If it ultimately proves useful for the treatment of neuropsychiatric disorders, TMS may well become a standard medical tool. The precise molecular mechanisms underlying the effects of TMS are unknown. Recent studies have measured monoamine release with microdialysis and imaging with raclopride after acute rTMS [11,12]. Recently, we described modulations in monoamine transporters following either acute or chronic rTMS [13]. However, there have been few reports of expression profiles following either acute or chronic rTMS. This prompted us to investigate the molecular effects of TMS in rodents by evaluating the expression of mouse genes after treatment with TMS. We found that the expression levels of dopamine receptor 2, HSP70, and several circadian rhythm-related genes were altered. And, a subsequent decrease in food and water intake were observed. In addition, our study showed that the binding of [^{3}H]raclopride was decreased after rTMS, suggesting that rTMS modulates D2 receptor gene expression and function, and it may be useful in the treatment of several neuropsychiatric disorders.

2. Materials and methods

2.1. Mice and conditions of rTMS

Male C57Black R6 mice (8 weeks old, 20–25 g) were chronically treated for 20 days (n = 42) or acutely for 1 day (n = 24) with rTMS. Mice were housed in a light-controlled room (8:00 a.m. on, 8:00 p.m. off). Stimulation was performed using a round-coil (7.5 cm

* Corresponding author at: Clinical Immunology, Institute of Medical Science, The University of Tokyo, 4-6-1 Shirokanedai, Minato-ku, Tokyo 108-8639, Japan.
E-mail address: ikedate4@ims.u-toyko.ac.jp (T. Ikeda).

0006-291X/$ - see front matter © 2013 Published by Elsevier Inc.
http://dx.doi.org/10.1016/j.bbrc.2013.03.017

outer diameter) and a Nihon Kohden Rapid Rate Stimulator (Nihon Kohden, Japan). Stimulation conditions were as follows: 20 Hz, 2 s; 20 times/day; inter-stimulus interval 1 min (30% machine output, representing about 0.75 T). The coil was placed over the head without touching the skull. Sham control mice were stimulated from a distance of more than 10 cm from the head. rTMS did not produce either notable seizures or changes in behavior, such as excessive struggling. Twenty-four hours after the last stimulation, the animals were sacrificed and their brains were processed for further analysis.

2.2. RNA extraction

Whole mouse brain was divided at the midbrain into cerebrum and cerebellum with brain stem (CBS). Total RNA was isolated from cerebrum and CBS by acid–phenol extraction [14]. Poly(A)+ RNA was isolated from the samples using an mRNA purification kit (TaKaRa Bio, Japan). Expression analysis by TaqMan real-time RT-PCR. We synthesized the TaqMan primer and probe sets with Primer Express Software (Applied Biosystems, Foster City, CA). The nucleotide sequence of the primers is shown in Supplementary data 3. Contaminating genomic DNA was removed with RNase-free DNase I (TaKaRa Bio, Japan). Complementary DNAs were synthesized using MMLV Reverse Transcription Reagents (Invitrogen, Carlsbad, CA). We used 1 μg of mRNA for the 100 μl reaction. The TaqMan PCR was performed as follows. We used 15 μl of TaqMan Universal PCR Master Mix (Applied Biosystems) in a 30 μl reaction. Primers and probes in optimal concentrations were added. We used 1 μl of RT mix for each PCR. Each sample was amplified in duplicate and the experiment was repeated at least three times. PCR conditions were standard for the 7700 Sequence Detector System (Applied Biosystems): 2 min at 50 °C, 10 min at 95 °C followed by 40 cycles of 95 °C for 15 s, 60 °C for 1 min. The mRNA quantity for the gene of interest was normalized by the quantity of GAPDH in each sample.

2.3. Ligand binding assay for dopamine receptor 2

Synaptosomes were prepared as previously described [15], using ice-cold buffer (50 mMTris–HCl, 120 mM NaCl, and 5 mM KCl) and incubated for 4 h at 4 °C with [3H]raclopride (3063.6 Gbq/mmol Perkin–Elmer), in binding buffer (50 mM Tris–HCl, 300 mM NaCl, and 5 mM KCl) containing 10 μM 7-OH-DPAT (Sigma) and 10 μM PD168077 (Sigma). Synaptosomes were washed four times rapidly with ice-cold buffer using filters (Whatman GF/B) for removal of excess radioligands, and any radioactivity remaining in the filters was measured by liquid scintillation spectrometry. Nonspecific uptake was determined in the presence of 10 μM raclopride (Sigma).

2.4. Cell culture

Neuro2a cells were maintained in Dulbecco's modified Eagle's medium supplemented with 10% fetal calf serum (FCS) at 37 °C under 5% CO2/95% air. Cells at subconfluence were harvested, diluted in culture medium, and plated in a 24-well culture plate for the uptake assay or in a 25 cm^2 culture flask for total RNA extraction. The cells were cultured with or without daily stimulation of chronic rTMS. And then, in the Neuro2a cellular model of Huntington disease [16], in which tNhtt-EGFP expression is induced and cells are

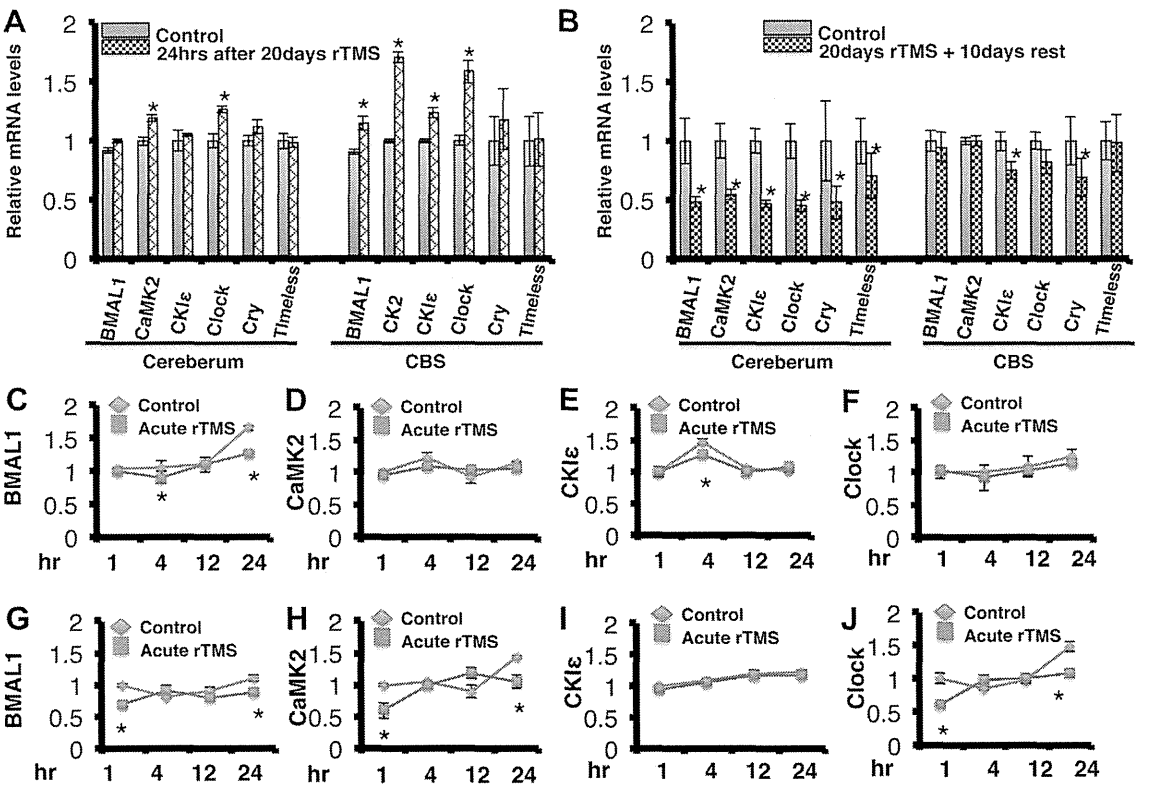

Fig. 1. Effects of rTMS on circadian rhythm related genes expression. (A, B) Effects of rTMS on circadian rhythm related genes mRNA levels. Mouse brains were treated by rTMS. The mRNA level was determined at 24 h and 10 days after 20 days rTMS stimulation. (C–F) Effects of acute rTMS on circadian rhythm related genes mRNA levels. Measurement were done at 1, 4, 12, 24 h after acute stimulation on cereberum. (G–J) Effects of acute rTMS on circadian rhythm related genes mRNA levels. Measurement were done at 1, 4, 12, 24 h after acute stimulation on CBS. mRNA level was compensated by GAPDH. Values represent means ± SEM of five experiments each performed in triplicate. *Significantly different from control at $P < 0.05$.

differentiated. Viability of tNhtt-150Q–EGFP cells was evaluated by MTT assay [16].

2.5. DNA chip profiling

We carried out comprehensive analysis of the altered gene expression in the cerebrum and CBS stimulated by chronic rTMS using a high-density oligonucleotide array (GeneChip; Affymetrix, Santa Clara, CA, USA), which has been described elsewhere [17]. Using the Affymetrix algorithm [18] and multiple analysis comparison software for assessing gene expression differences, mRNAs that were increased or decreased in the mouse brain with chronic rTMS stimulation relative to levels in control mouse brain were identified.

2.6. Western blotting and immunocytochemistry

Cells were washed with phosphate-buffered saline and treated with Laemmli sample buffer. Western blotting and immunocytochemistry were performed as described previously [16]. Mouse monoclonal anti-Hsp70 (SPA-810) were purchased from StressGen Biotechnologies (Victoria, British Columbia).

2.7. Data analysis

The data were represented as means ± SE of at least three independent experiments, each performed in triplicate or duplicate. Statistical analysis was performed using ANOVA (Fig. 1) and Student's *t*-test as appropriate.

3. Results

3.1. Changes in the expression of genes in the mouse brain after rTMS

We stimulated the brains of 8-week-old C57 Black mice for 20 days with rTMS and analyzed the changes in the expression of genes in mice brains that were stimulated by acute and chronic rTMS with an Affymetrix GeneChip microarray, and we found that the mRNA of many genes, including HSP70, dopamine receptor 2, and circadian-related genes, were altered in the cerebrum and CBS (Supplementary data 1 and 2). In order to evaluate the effects of rTMS on these genes, we measured the mRNA levels of several genes with RT-PCR (Tables 1–3).

3.2. Effects of acute and chronic rTMS on circadian rhythm-related genes

The GeneChip data showed that Period 2 mRNA levels were decreased after rTMS. Thus, we examined the mRNA levels of circadian-related genes at 24 h after 20 days of rTMS and after 10 days of rest after 20 days of rTMS. Twenty-four hours after 20 days of rTMS, Period 3, BMAL1, Calmodulin kinase II (CaMK2), casein kinase 1ε (CK-1ε), and Clock mRNA levels were increased in CBS, and CaMK2 and Clock mRNA levels were increased in the cerebrum (Table 2, Fig. 1A). However, Period 2 mRNA levels were

Table 1
Summary of gene expression profile by rTMS stimulation.

			20 days + 24 days	20 days + 10 days	1 h	4 h	12 h	24 h
RhoG	Cereberum	Mg+	0.705 ± 0.057[a]	1.094 ± 0.044	1.053 ± 0.47	0.721 ± 0.183[a]	0.903 ± 0.309	1.2 ± 0.129[a]
		Control	1.05 ± 0.059	1.137 ± 0.056	0.938 ± 0.418	0.89 ± 0.225	1.005 ± 0.139	1.0 ± 0.16
	CBS	Mg+	0.929 ± 0.015	0.824 ± 0.087[a]	0.913 ± 0.185	0.859 ± 0.198[a]	1.159 ± 0.285	0.83 ± 0.096
		Control	1.0 ± 0.08	1.0 ± 0.033	1.005 ± 0.231	1.3 ± 0.321	1.26 ± 0.309	0.87 ± 0.23
Periodl	Cereberum	Mg+	0.979 ± 0.014	0.848 ± 0.029[a]	1.927 ± 0.071[a]	1.429 ± 0.065[a]	1.581 ± 0.015	1.972 ± 0.141
		Control	1.002 ± 0.05	1.00 ± 0.013	0.992 ± 0.011	2.081 ± 0.113	1.511 ± 0.026	2.128 ± 0.051
	CBS	Mg+	1.254 ± 0.052	0.712 ± 0.027[a]	1.761 ± 0.036[a]	1.356 ± 0.011	2.432 ± 0.078	2.552 ± 0.134[a]
		Control	1.00 ± 0.018	1.00 ± 0.012	1.0 ± 0.024	1.465 ± 0.022	2.184 ± 0.041	1.875 ± 0.046
Period2	Cereberum	Mg+	0.601 ± 0.022[a]	0.764 ± 0.162[a]	1.176 ± 0.84	0.429 ± 0.159[a]	0.748 ± 0.325	0.796 ± 0.268
		Control	1.0 ± 0.056	1.0 ± 0.238	1.0 ± 0.937	0.688 ± 0.231	0.791 ± 0.374	0.756 ± 0.062
	CBS	Mg+	0.411 ± 0.128[a]	1.107 ± 0.27	1.08 ± 0.103	0.635 ± 0.074	1.457 ± 0.084	0.919 ± 0.055
		Control	1.0 ± 0.124	1.0 ± 0.062	1.08 ± 0.077	0.61 ± 0.094	1 457 ± 0.084	0.955 ± 0.05
Period3	Cereberum	Mg+	0.943 ± 0.012	0.929 ± 0.05	0.968 ± 0.071	1.295 ± 0.141	1.082 ± 0.035	1.347 ±0.12[a]
		Control	1.0 ± 0.047	1.0 ± 0.058	1.0 ± 0.071	1.494 ± 0.068	1.263 ± 0.127	0.985 ± 0.047
	CBS	Mg+	1.404 ± 0.026[a]	0.887 ± 0.096	0.875 ± 0.06	1.438 ± 0.047	1.396 ± 0.065	1.417 ± 0.032
		Control	1.0 ± 0.047	1.0 ± 0.0556	1.0 ± 0.062	1.300 ± 0.073	1.301 ± 0.089	1.429 ± 0.024
D-E-A-D	Cereberum	Mg+	0.913 ± 0.044	0.983 ± 0.137	1.545 ± 0.948	1.279 ± 0.228	1.457 ± 0.669	1.227 ± 0.176
		Control	1.0 ± 0.07	1.0 ± 0.203	1.0 ± 0.305	0.869 ± 0.258	1.112 ± 0.529	1.211 ± 0.28
	CBS	Mg+	1.519 ± 0.101[a]	1.096 ± 0.184	1.061 ± 0.125	1.300 ± 0.171[a]	1.1182 ± 0.136[a]	1.086 ± 0.061[a]
		Control	1.0 ± 0.04	1.0 ± 0.238	1.0 ± 0.255	2.255 ± 0.438	1.607 ± 0.223	1.244 ± 0.045
Dr-1	Cereberum	Mg+	0.689 ± 0.046[a]	1.066 ± 0.196	0.627 ± 0.241[a]	0.542 ± 0.061	0.693 ± 0.046	0.661 ± 0.171
		Control	1.0 ± 0.054	1.0 ± 0.144	1.0 ± 0.573	0.497 ± 0.054	0.594 ± 0.091	0.542 ± 0.187
	CBS	Mg+	0.992 ± 0.057	1.012 ± 0.116	1.023 ± 0.437	0.865 ± 0.159	0.991 ± 0.267	0.703 ± 0.192
		Control	1.0 ± 0.061	1.0 ± 0.148	1.0 ± 0.213	1.126 ± 0.664	0.964 ± 0.423	0.771 ± 0.237
IGF1 receptor	Cereberum	Mg+	0.819 ± 0.044	0.598 ± 0.069[a]	0.997 ± 0.023	1.028 ± 0.106	1.202 ± 0.075	1.143 ± 0.069
		Control	1.0 ± 0.121	1.0 ± 0.131	1.0 ± 0.041	1.191 ± 0.076	1.271 ± 0.092	1.198 ± 0.07
	CBS	Mg+	1.122 ± 0.216	0.744 ± 0.065	1.039 ± 0.007	0.927 ± 0.068	1.616 ± 0.122	2.050 ± 0.08
		Control	1.0 ± 0.145	1.0 ± 0.095	1.0 ± 0.05	1.046 ± 0.026	1.721 ± 0.097	2.186± 0.15
Cry1	Cereberum	Mg+			1.145 ± 0.08[a]	1.439 ± 0.166	1.182 ± 0.05 [a]	1.340 ± 0.141
		Control			1.0 ± 0.051	1.621 ± 0.11	1.367 ± 0.15	1.425 ± 0.244
	CBS	Mg+			1.103 ± 0.176	1.528 ± 0.532	1.56 ± 0.606*	2.029 ± 0.403 *
		Control			1.0 ± 0.293	1.293 ± 0.172	2.058 ± 0.094	1.663 ± 0.226
Timeless	Cereberum	Mg+			0.845 ± 0.04[a]	0.947 ± 0.104	1.007 ± 0.096	1.122 ± 0.134
		Control			1.0 ± 0.077	1.035 ± 0.006	1.093 ± 0.094	1.039 ± 0.134
	CBS	Mg+			0.613 ± 0.194[a]	0.859 ± 0.18 [a]	1.170 ± 0.273	1.151 ± 0.208
		Control			1.0 ± 0.274	1.039 ± 0.059	1.218 ± 0.252	1.310 ± 0.417

Values represent means ± SEM of three experiments each performed in triplicate.
[a] Significantly different from control at $P < 0.05$.

Table 2
Summary of gene expression profile by rTMS stimulation.

			20 days + 24 days	20 days + 10 days	1 h	4 h	12 h	24 h
AMPA	Cereberum	Mg+	0.926 + 0.128	1.028 + 0.244	0.546 + 0.081[a]	0.683 + 0.098[a]	0.982 + 0.156	0.653 + 0.149
		Control	1.0 + 0.051	1.0 + 0.162	1.0 + 0.4	1.634 + 0.523	0.987 + 0.21	0.656 + 0.23
	CBS	Mg+	1.459 + 0.083[a]	1.151 + 0.104[a]	0.071 + 0.06[a]	0.198 + 0.391[a]	0.571 + 1.574[a]	0.210 + 0.388[a]
		Control	1.0 + 0.089	1.0 + 0.08	1.0 + 2.024	0.963 + 1.653	0.295 + 0.733	0.135 + 0.264
NMDA1	Cereberum	Mg+	0.892 + 0.109	0.911 + 0.286	1.176 + 0.84	0.429 + 0.159[a]	0.748 + 0.325	0.796 + 0.268
		Control	1.008 + 0.038	1.0 + 0.115	1.0 + 0.937	0.689 + 0.231	0.791 + 0.374	0.756 + 0.062
	CBS	Mg+	0.816 + 0.119	1.4 + 0.259[a]	1.063 + 0.017[a]	0.954 + 0.122	1.075 + 0.027	0.834 + 0.02 [a]
		Control	1.0 + 0.016	1.095 + 0.152	1.0 + 0.036	1.134 + 0.183	1.119 + 0.058	0.995 + 0.057
5HT 1b	Cereberum	Mg+	1.337 + 0.008[a]	1.39 + 0.071[a]	1.150 + 0.047	1.408 + 0.197	1.203 + 0.048	1.136 + 0.013
		Control	1.0 + 0.016	1.057 + 0.057	1.0 + 0.008	1.667 + 0.117	1.135 + 0.084	1.173 + 0.043
	CBS	Mg+	1.836 + 0.051[a]	0.861 + 0.123	0.552 + 0.055	0.933 + 0.173	1.116 + 0.082	1.110 + 0.176
		Control	1.0 + 0.016	1.0 + 0.076	1.0 + 0.33	0.734 + 0.068	0.992 + 0.267	1.124 + 0.072
5HT4	Cereberum	Mg+	1.19 + 0.014[a]	1.240 + 0.101[a]	0.969 + 0.023	1.272 + 0.112	1.074 + 0.037	1.380 + 0.055[a]
		Control	1.0 + 0.025	1.0 + 0.141	1.0 + 0.032	1.345 + 0.093	1.116 + 0.04	1.169 + 0.025
	CBS	Mg+	1.886 + 0.01[a]	0.923 + 0.044	0.841 + 0.068	0.94 + 0.069[a]	0.69 + 0.087	0.824 + 0.172
		Control	1.0 + 0.005	1.0 + 0.007	1.006 + 0.214	0.614 + 0.022	0.714 + 0.11	0.694 + 0.05
5HT7	Cereberum	Mg+	1.240 + 0.03	1.136 + 0.035[a]	0.905 + 0.024[a]	1.204 + 0.058	0.911 + 0.015	1.0 + 0.009
		Control	1.0 + 0.016	1.0 + 0.017	1.0 + 0.014	1.334 + 0.075	1.036 + 0.042	1.039 + 0.043
	CBS	Mg+	1.682 + 0.01[a]	0.986 + 0.029	0.972 + 0.047	0.947 + 0.032[a]	1.036 + 0.013	1.054 + 0.066
		Control	1.0 + 0.022	1.0 + 0.051	1.0 + 0.036	1.049 + 0.017	1.082 + 0.067	1.042 + 0.041
Ab3	Cereberum	Mg+	0.936 + 0.039	0.937 + 0.065	0.817 + 0.028[a]	1.159 + 0.042	0.777 + 0.023	0.884 + 0.032[a]
		Control	1.0 + 0.018	1.0 + 0.05	1.0 + 0.038	1.201 + 0.061	0.883 + 0.036	0.587 + 0.028
	CBS	Mg+	0.978 + 0.004	0.877 + 0.033	1.129 + 0.043	0.965 + 0.004[a]	0.948 + 0.025[a]	0.597 + 0.025
		Control	1.0 + 0.005	1.0 + 0.046	1.0 + 0.031	0.908 + 0.004	0.658 + 0.017	0.591 + 0.031
Ca channel	Cereberum	Mg+	1.032 + 0.007	1.025 + 0.014	1.006 + 0.03	1.298 + 0.066[a]	1.068 + 0.008[a]	1.232 + 0.028
		Control	1.0 + 0.029	1.0 + 0.023	1 + 0.015	1.636 + 0.02	1.183 + 0.014	1.133 + 0.028
	CBS	Mg+	0.689 + 0.01[a]	0.990 + 0.047	0.891 + 0.003[a]	1.015 + 0.019[a]	1.386 + 0.022[a]	1.448 + 0.02
		Control	1.0 + 0.027	1.0 + 0.019	1.0 + 0.011	1.242 + 0.03	1.173 + 0.013	1.386 + 0.039
Cl channel	Cereberum	Mg+	987 + 0.023	1.184 + 0.147	0.803 + 0.03	0.960 + 0.048	0.799 + 0.005[a]	1.041 + 0.003
		Control	1.0 + 0.018	1.0 + 0.14	1.0 + 0.039	0.927 + 0.036	0.91 + 0.013	1.031 + 0.04
	CBS	Mg+	1.238 + 0.014[a]	0.936 + 0.14	0.387 + 0.155[a]	0.628 + 0.087	0.697 + 0.157	0.705 + 0.022[a]
		Control	1.0 + 0.031	1.0 + 0.058	1.0 + 0.521	0.570 + 0.066	0.890 + 0.344	0.843 + 0.027
D2	Cereberum	Mg+	0.565 + 0.01	1.273 + 0.066	1.011 + 0.016	1.276 + 0.029	1.087 + 0.008	1.188 + 0.013
		Control	1.0 + 0.009	1.0 + 0.071	1.0 + 0.003	1.423 + 0.041	1.151 + 0.014	1.236 + 0.031
	CBS	Mg+	0.772 + 0.01[a]	0.763 + 0.016[a]	0.688 + 0.012	0.728 + 0.01	1.010 + 0.027	0.915 + 0.012
		Control	1.0 + 0.002	1.0 + 0.009	1.0 + 0.066	0.640 + 0.007	0.816 + 0.028	0.783 + 0.018
D4	Cereberum	Mg+	1.198 + 0.031	1.278 + 0.057	0.651 + 0.089[a]	0.963 + 0.023[a]	0.454 + 0.015[a]	0.644 + 0.02
		Control	1.0 + 0.023	1.0 + 0.071	1.0 + 0.05	0.687 + 0.037	0.648 + 0.058	0.706 + 0.061
	CBS	Mg+	0.924 + 0.036	0.684 + 0.206[a]	0.845 + 0.09	0.914 + 0.129[a]	1.190 + 0.168	0.895 + 0.202[a]
		Control	1.0 + 0.005	1.0 + 0.165	1.0 + 0.376	0.579 + 0.09	1.254 + 0.316	0.468 + 0.08
GABA A3	Cereberum	Mg+	1.11 + 0.012	3.22 + 0.235[a]	0.901 + 0.037	1.240 + 0.226	0.972 + 0.055	1.20 + 0.079[a]
		Control	1.047 + 0.064	1.0 + 0.016	1.0 + 0.081	1.2 + 0.108	0.972 + 0.045	0.998 + 0.124
	CBS	Mg+	1.314 + 0.015[a]	1.456 + 0.278	0697 + 0.017	0.955 + 0.053[a]	1.098 + 0.026	0.896 + 0.049
		Control	1.0 + 0.009	1.0 + 0.266	1.0 + 0.116	0.684 + 0.008	0.992 + 0.069	0.857 + 0.022

Values represent means ± SEM of three experiments each performed in triplicate.
[a] Significantly different from control at $P < 0.05$.

decreased in the cerebrum and CBS (Table 2). After 10 days of rest after 20 days of rTMS treatment, Period 1, Period 2, BMAL1, CaMK2, CKIε, Clock, Cry1, and Timeless mRNA levels were decreased in the cerebrum, and Period 1, CK1ε, and Cry mRNA levels were decreased in CBS. There were no changes in Period 3 mRNA levels (Table 2, Fig. 1B). Next, we examined the acute effects of rTMS at 1, 4, 12, and 24 h. After acute rTMS, BMAL1 mRNA levels were decreased in the cerebrum at 4 and 24 h after acute rTMS (Fig. 1C) and in CBS at 1 and 24 h after acute rTMS (Fig. 1D). After acute rTMS, CaMK2 mRNA levels did not change in the cerebrum (Fig. 1D), but they were decreased after 1 and 24 h in CBS (Fig. 1H). CKIε mRNA levels were decreased in the cerebrum at 4 h after acute rTMS, (Fig. 1E) but they were not changed in CBS (Fig. 1I). Clock mRNA levels were not changed after acute rTMS in the cerebrum (Fig. 1F), but they were decreased in CBS at 1 and 24 h (Fig. 1J). Cry1 mRNA levels were upregulated at 1 h and decreased at 12 h in the cerebrum (Table 2); however, in CBS (Table 2), Cry1 mRNA levels were decreased at 12 h and upregulated at 24 h. Timeless mRNA levels were decreased 1 h after acute rTMS in the cerebrum (Table 2), and they were decreased at 1 and 4 h after acute rTMS in CBS (Table 2).

These findings suggested that the changes induced by rTMS in the mRNA expression patterns of the circadian rhythm-related genes may have some effects on neuropsychiatric disorders.

3.3. Effects of rTMS on water and food intake

Chronic rTMS changed the mRNA levels of the circadian rhythm-related genes. Thus, we examined whether chronic rTMS altered food and water intake. There were no changes in water and food intake at night (8:00 PM–8:00 AM) (Fig. 2A and B). However, in the daytime (8:00 AM–8:00 PM), rTMS inhibited water and food intake on days 14–20 and 15–20 (Fig. 2C and D).

3.4. Effects of acute and chronic rTMS on HSP70 induction

From the GeneChip data, we found that Heat Shock protein-related genes were altered (Supplementary data 1 and 2). Thus, we examined the effects of acute and chronic rTMS on HSP70 induction. The effects of rTMS on HSP70 induction were examined with tNhtt-150Q-EGFP cells and in the cerebrum and CBS. HSP70 mRNA and protein levels were increased after 5, 10, and 20 days of rTMS

Table 3
Summary of gene expression profile by rTMS stimulation.

			20 davs + 24 davs	20 davs + 10 davs	1 h	4 h	12 h	24 h
GABAb2	Cereberum	Mg+	1.203 + 0.036	1.20 + 0.064[a]	0.980 + 0.046	1.079 + 0.256	0.779 + 0.05[a]	1.082 + 0.085
		Control	1.0 + 0.107	1.0 + 0.037	1.0 + 0.17	0.891 + 0.088	0.864 + 0.046	1.044 + 0.232
	CBS	Mg+	1.618 + 0.034	1.167 + 0.108	0.452 + 0.017[a]	1.077 + 0.066	1.206 + 0.086	1.336 + 0.191[a]
		Control	1.0 + 0.051	1.0 + 0.057	1.0 + 0.176	1.075 + 0.092	1.210 + 0.014	1.921 + 0.163
NA channelbl	Cereberum	Mg+	0.951 + 0.019	1.074 + 0.032	0.870 + 0.014[a]	1.070 + 0.052	0.906 + 0.028	1.10 + 0.02[a]
		Control	1.0 + 0.026	1.0 + 0.043	1.0 + 0.008	1.230 + 0.028	1.004 + 0.035	0.864 + 0.002
	CBS	Mg+	1.022 + 0.03	1.025 + 0.065	0.816 + 0.05[a]	0.852 + 0.011[a]	1.077 + 0.019	1.043 + 0.085[a]
		Control	1.0 + 0.034	1.0 + 0.035	1.0 + 0.07	1.011 + 0.073	1.090 + 0.099	1.217 + 0.083
Opioid kappa	Cereberum	Mg+	0.961 + 0.008	1.044 + 0.047	0.936 + 0.012	1.141 + 0.04	0.923 + 0.008	1.014 + 0.013
		Control	1.0 + 0.031	1.0 + 0.021	1.0 + 0.008	1.048 + 0.017	1.002 + 0.018	1.021 + 0.034
	CBS	Mg+	1.5 + 0.005 [a]	0.969 + 0.014	0.633 + 0.007	0.792 + 0.022	0.873 + 0.025	0.708 + 0.022[a]
		Control	1.0 + 0.002	1.0 + 0.009	1.0 + 0.055	0.845 + 0.011	0.863 + 0.02	1.091 + 0.042
TSH	Cereberum	Mg+	0.816 + 0.015	1.191 + 0.221	0.943 + 0.067	1.240 + 0.046	0.690 + 0.021[a]	1.01 + 0.053
		Control	1.0 + 0.068	1.0 + 0.369	1.0 + 0.055	1.272 + 0.167	0.953 + 0.024	1.125 + 0.063
	CBS	Mg+	1.093 + 0.017	0.753 + 0.32	0.491 + 0.284[a]	0.938 + 0.449	0.518 + 0.171	0.637 + 0.443
		Control	1.0 + 0.021	1.0 + 0.245	1.0 + 0.192	0.631 + 0.157	0.535 + 0.389	0.518 + 0.332
HSP70	Cereberum	Mg+	0.852 + 0.076	0.987 + 0.041	1.23 + 0.248[a]	0.468 + 0.074	0.876 + 0.641	0.524 + 0.061
		Control	1.053 + 0.101	1.0 + 0.06	1.0 + 0 .201	0.656 + 0.322	0.676 + 0.073	0.484 + 0.091
	CBS	Mg+	0.765 + 0.037	1.099 + 0.076	1.951 + 0.322[a]	0.692 + 0.114[a]	1.027 + 0.069	0.585 + 0.062
		Control	1.0 + 0.136	1.0 + 0.052	1.0 + 0.106	1.295 + 0.592	1.124 + 0.223	0.691 + 0.146
HAP1	Cereberum	Mg+	0.940 + 0.055	0.950 + 0.08	1.047 + 0.408	0.680 + 0.09	0.819 + 0.218	0.92 + 0.056[a]
		Control	1.0 + 0.039	1.0 + 0.121	1.0 + 0.638	0.679 + 0.189	0.869 + 0.117	0.713 + 0.192
	CBS	Mg+	0.813 + 0.085	1.421 + 0.329	0.979 + 0.064	1.105 + 0.101[a]	1.097 + 0.127	1.023 + 0.003[a]
		Control	1.0 + 0.055	1.0 + 0.041	1.0 + 0.095	1.6 + 0.21	1.323 + 0.1	1.164 + 0.013
Tau	Cereberum	Mg+	0.759 + 0.083	1.029 + 0.147	0.91 + 0.637	0.574 + 0.208	0.764 + 0.47	0.694 + 0.146
		Control	1.0 + 0.026	1.0 + 0.113	1.0 + 0.995	0.850 + 0.3	0.832 + 0.138	0.589 + 0.139
	CBS	Mg+	1 330 + 0 087[a]	0.914 + 0.17	0.975 + 0.261	0.324 + 0.09[a]	0.408 + 0.289	0.291 + 0.056[a]
		Control	1.0 + 0.037	1.0 + 0.196	1.0 + 0.115	0.679 + 0.492	0.501 + 0.265	0.337 + 0.101
CUGBP	Cereberum	Mg+	0.861 + 0.061	0.906 + 0.078	1.062 + 0.74	0.641 + 0.185	0.637 + 0.154[a]	0.848 + 0.134[a]
		Control	1.0 + 0.022	1.0 + 0.134	1.0 + 0.971	0.697 + 0.229	0.819 + 0.07	0.631 + 0.184
	CBS	Mg+	1.258 + 0.08[a]	0.985 + 0.078	0.678 + 0.142[a]	0.837 + 0.169[a]	1.021 + 0.182	0.824 + 0.115
		Control	1.0 + 0.089	1.0 + 0.15	1.0 + 0.124	1.633 + 0.469	1.123 + 0.349	0.723 + 0.182
Caspase3	Cereberum	Mg+	0.731 + 0.037[a]	0.898 + 0.027	1.032 + 0.552	0.677 + 0.163	0.889 + 0.294	0.937 + 0.129[a]
		Control	1.0 + 0.088	1.0 + 0.06	1.0 + 0.649	0.696 + 0.064	0.832 + 0.099	0.721 + 0.179
	CBS	Mg+	1.022 + 0.055	0.985 + 0.028	0.889 + 0.213	0.997 + 0.177[a]	1.009 + 0.219[a]	0.989 + 0.181
		Control	1.0 + 0.063	1.0 + 0.057	1.0 + 0.209	1.285 + 0.39	1.299 + 0.326	1.055 + 0.137
SKD3	Cereberum	Mg+	0.938 + 0.019	1.081 + 0.063[a]	0.839 + 0.035[a]	1.126 + 0.08[a]	1.173 + 0.044	1.351 + 0.094
		Control	1.0 + 0.074	1.0 + 0.048	1.0 + 0.041	1.337 + 0.022	1.181 + 0.084	1.318 + 0.079
	CBS	Mg+	1.271 + 0.046[a]	1.126 + 0.058	0.665 + 0.028[a]	1.038 + 0.02	1.328 + 0.061	1.125 + 0.002[a]
		Control	1.0 + 0.044	1.0 + 0.024	1.0 + 0.057	1.195 + 0.115	1.217 + 0.05	1.503 + 0.117
TransG	Cereberum	Mg+	0.970 + 0.009	1.040 + 0.037	1.274 + 0.064[a]	0.950 + 0.009	0.862 + 0.064	0.924 + 0.04[a]
		Control	1.0 + 0.018	1.0 + 0.021	1.0 + 0.041	0.933 + 0.059	0.765 + 0.011	1.195 + 0.055
	CBS	Mg+	1.033 + 0.19	0.831 + 0.63	1.047 + 0.51	0.861 + 0.47	1.311 + 0.107	0.882 + 0.007
		Control	1.0 + 0.29	1.0 + 0.37	1.0 + 0.17	1.064 + 0.34	1.023 + 0.34	1.199 + 0.062
ATM	Cereberum	Mg+	0.772 + 0.026[a]	0.746 + 0.292[a]	0.888 + 0.114	0.880 + 0.199[a]	0.992 + 0.049[a]	0.992 + 0.065[a]
		Control	1.0 + 0.079	1.0 + 0.152	1.0 + 0.024	1.138 + 0.098	1.202 + 0.035	1.146 + 0.058
	CBS	Mg+	1.491 + 0.087[a]	1.088 + 0.217	0.947 + 0.271	0.883 + 0.084	1.114 + 0.226	0.907 + 0.082
		Control	1.0 + 0.097	1.0 + 0.194	1.0 + 0.212	1.548 + 0.493	1.615 + 1.195	0.960 + 0.194

Values represent means ± SEM of three experiments each performed in triplicate.
[a] Significantly different from control at $P < 0.05$.

in the tNhtt-150Q–EGFP cells (Fig. 3A, B and C). Because HSP70 is known to cure the misfoldings of the 150Q aggregate, we investigated whether 20 days of rTMS increased the cell viability of the tNhtt-150Q-EGFP cells. Twenty days of rTMS increased cell viability compared with controls (Fig. 3). In the mouse brain, acute rTMS increased HSP70 mRNA levels at 1 h and thereafter. However, no HSP70 mRNA changes were observed after 20 days of rTMS (Table 3).

3.5. Effects of rTMS on dopamine receptor 2

From the GeneChip data, we found that dopamine receptor 2 mRNA levels were changed. Therefore, we investigated dopamine receptor 2 mRNA levels and protein function after rTMS. We found that chronic rTMS decreased the mRNA levels of the D2 receptor, but no changes were found with acute rTMS (Table 3). In order to confirm these effects, we used a [^{3}H]ligand-binding assay of synaptosomes of the whole brain that were collected 24 h after mice were treated with rTMS for 20 days. We verified that [^{3}H]raclopride binding was decreased. A decrease in the B_{max} and no change in the K_D of [^{3}H]raclopride binding was observed in the binding assay (K_D: rTMS-treated, 14.74 ± 4.684 nM; control, 13.39 ± 5.219 nM; B_{max}: rTMS-treated, 4026 ± 305 fmol/μg of protein/min; control, 6296 ± 417 fmol/μg of protein/min) (Fig. 4).

4. Discussion

rTMS has been widely used to treat neuropsychiatric disorders. However, the underlying mechanisms of this treatment are not clear. In order to study the effects of chronic rTMS, we treated mice brains with a chronic rTMS protocol for 20 days. We have previously shown that acute and chronic rTMS alters monoamine transporter (MAT) mRNA, protein levels, and function [13]. In order to investigate the changes in gene expression that were induced by rTMS, we performed a GeneChip analysis. From these data (Supplementary data 1 and 2), we confirmed changes in some of the MAT-related genes.

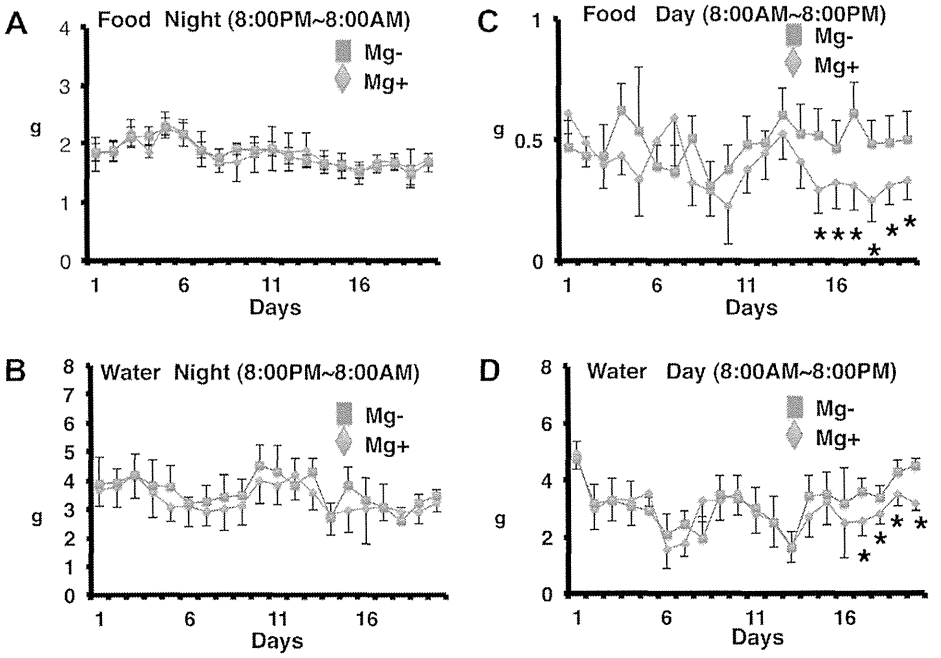

Fig. 2. Effects of rTMS on food and water intake. (A, C) Effects of rTMS on food intake. The weight of food intake was determined at 8:00 AM (A) and 8:00 PM (C). (B, D) Effects of rTMS on water uptake. The weight of water intake was determined at 8:00 AM (B) and 8:00 PM (D). Values represent means ± SEM of five experiments each performed in triplicate. *Significantly different from control at $P < 0.05$.

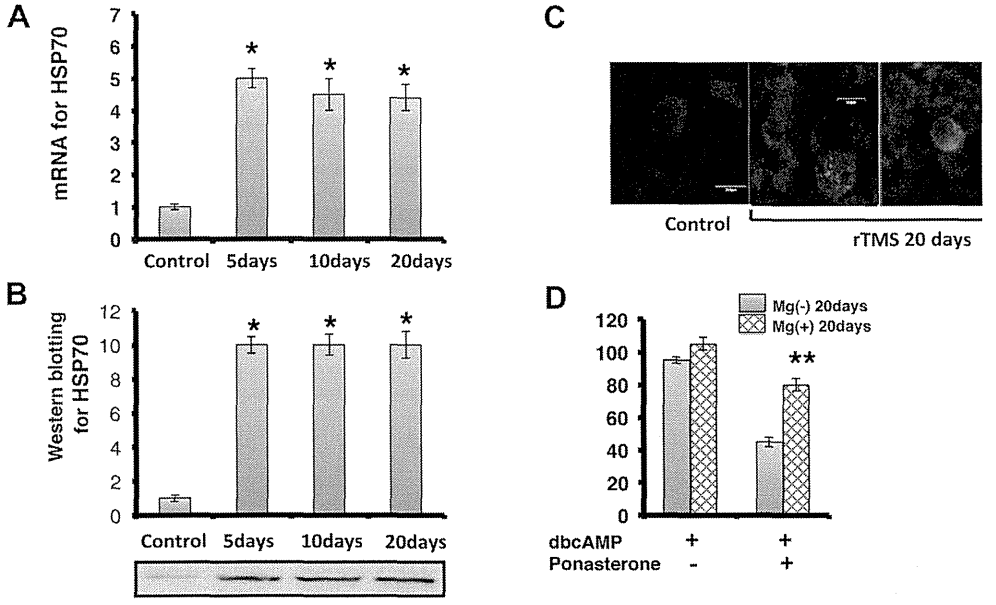

Fig. 3. Effects of rTMS on HSP70 mRNA and protein levels. (A–C) Effects of rTMS on HSP70 mRNA and protein levels. tNhtt-150Q–EGFP cells were treated by rTMS. The mRNA and protein level was determined at 24 h after stimulation. (D) Viability of tNhtt-150Q–EGFP cells stimulated by rTMS. Values represent means ± SEM of three experiments each performed in triplicate. *Significantly different from control at $P < 0.05$. **$P < 0.01$ versus control treatment with ponasterone A and dbcAMP.

We found that HSP70 mRNA and protein levels were increased in tNhtt-150Q-EGFP cells by chronic rTMS and in mouse cerebrum by acute rTMS. In addition, 20 days of rTMS increased the cell viability of tNhtt-150Q-EGFP cells. These results indicated that rTMS may result in improvement in patients with Huntington's diseases through the induction of HSP70. Further investigations are needed regarding the effects of chronic rTMS because we observed that acute rTMS increased HSP70 mRNA levels, whereas there were no changes observed 24 h after 20 days of rTMS.

In addition, we found that dopamine receptor 2 and dopamine receptor 4 mRNA levels were decreased in mouse brain after chronic rTMS. Thus, we examined the D2 receptor function with a ligand-binding assay. Chronic rTMS decreased [^{3}H]raclopride binding (Fig. 4). Because D2 receptor agonists are now widely used to treat schizophrenia, chronic rTMS may result in improvement in patients with psychiatric disorders through the effects on the D2 receptor.

We also observed that chronic rTMS inhibited food and water intake during the daytime (Fig. 2). Recently, circadian rhythm-related transcription factors have been found. Thus, we investigated whether chronic rTMS altered the mRNA levels of circadian rhythm-related genes. After 20 days of rTMS, Period 2 mRNA levels

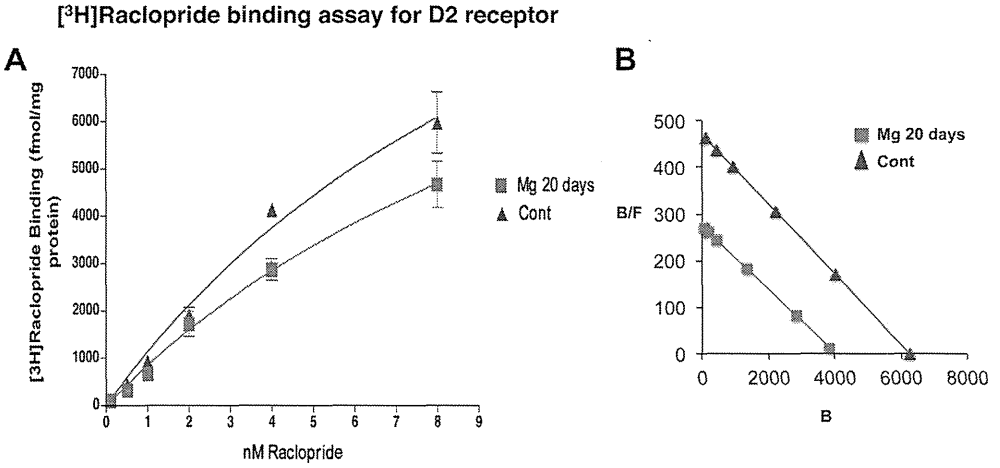

Fig. 4. Effects of chronic rTMS (20 days) on the binding of [^{3}H]raclopride in mouse brain. (A) raclopride binding assay-specific ligands for D2 receptor were evaluated using radiolabeled Raclopride. The Left panel shows the saturation analysis of [^{3}H]raclopride. Points and bars represent means ± SEM, $N = 3$. Right panel shows the Eadie–Hofstee plot of [^{3}H]raclopride binding. Each point represents the mean of three independent experiments obtained in (A, left panel). Values represent means ± SEM of three experiments each performed in duplicate.

were decreased in the cerebrum and CBS, whereas BMLA1, CaMK2, CKIε, and Clock mRNA levels were increased in CBS (CaMK2 and Clock were increased in the cerebrum too). These results indicated that circadian rhythm-related genes may be involved in the changes in the food and water intake that were induced by chronic rTMS.

Our results suggested the involvement of HSP70, the D2 receptor, and circadian rhythm-related gene expression changes in the therapeutic effects of chronic rTMS. Further research on the regulation of HSP70, the D2 receptor, and circadian rhythm-related gene expression by chronic rTMS will be needed in order to develop more effective rTMS therapies for the treatment of patients with neuropsychiatric disorders in which HSP70 and dopamine systems are involved. Moreover, it will be important to fine-tune the method or the apparatus to stimulate certain brain areas more specifically and reduce unnecessary side effects.

Acknowledgments

This work was supported partly by a grant from the JSPS (Japan Society for the Promotion of Science). This work was supported by Global COE Program "Center of Education and Research for the Advanced Genome-Based Medicine-For personalized medicine and the control of worldwide infectious disease-", MEXT Japan.

Appendix A. Supplementary data

Supplementary data associated with this article can be found, in the online version, at http://dx.doi.org/10.1016/j.bbrc.2013.03.017.

References

[1] A.T. Barker, I.L. Freeston, R. Jalinous, J.A. Jarratt, Magnetic stimulation of the human brain and peripheral nervous system: an introduction and the results of an initial clinical evaluation, Neurosurgery 20 (1987) 100–109.

[2] A. Post, M.E. Keck, Transcranial magnetic stimulation as a therapeutic tool in psychiatry: what do we know about the neurobiological mechanisms? Journal of Psychiatric Research 35 (2001) 193–215.

[3] M. Hallett, Transcranial magnetic stimulation and the human brain, Nature 406 (2000) 147–150.

[4] B.J. Roth, J.M. Saypol, M. Hallett, L.G. Cohen, A theoretical calculation of the electric field induced in the cortex during magnetic stimulation, Electroencephalography and Clinical Neurophysiology 81 (1991) 47–56.

[5] P.A. Merton, H.B. Morton, Stimulation of the cerebral cortex in the intact human subject, Nature 285 (1980) 227.

[6] M.S. George, E.M. Wassermann, R.M. Post, Transcranial magnetic stimulation: a neuropsychiatric tool for the 21st century, The Journal of Neuropsychiatry and Clinical Neurosciences 8 (1996) 373–382.

[7] T. Zyss, Deep magnetic brain stimulation–the end of psychiatric electroshock therapy?, Medical Hypotheses 43 (1994) 69–74

[8] T. Paus, J. Barrett, Transcranial magnetic stimulation (TMS) of the human frontal cortex: implications for repetitive TMS treatment of depression, Journal of Psychiatry & Neuroscience: JPN 29 (2004) 268–279.

[9] N. Dragasevic, A. Potrebic, A. Damjanovic, E. Stefanova, V.S. Kostic, Therapeutic efficacy of bilateral prefrontal slow repetitive transcranial magnetic stimulation in depressed patients with Parkinson's disease: an open study, Movement Disorders: Official Journal of the Movement Disorder Society 17 (2002) 528–532.

[10] M.S. George, S.H. Lisanby, H.A. Sackeim, Transcranial magnetic stimulation: applications in neuropsychiatry, Archives of General Psychiatry 56 (1999) 300–311.

[11] M. Kanno, M. Matsumoto, H. Togashi, M. Yoshioka, Y. Mano, Effects of acute repetitive transcranial magnetic stimulation on dopamine release in the rat dorsolateral striatum, Journal of the Neurological Sciences 217 (2004) 73–81.

[12] T. Ohnishi, T. Hayashi, S. Okabe, I. Nonaka, H. Matsuda, H. Iida, E. Imabayashi, H. Watabe, Y. Miyake, M. Ogawa, N. Teramoto, Y. Ohta, N. Ejima, T. Sawada, Y. Ugawa, Endogenous dopamine release induced by repetitive transcranial magnetic stimulation over the primary motor cortex: an [11C]raclopride positron emission tomography study in anesthetized macaque monkeys, Biological Psychiatry 55 (2004) 484–489.

[13] T. Ikeda, M. Kurosawa, C. Uchikawa, S. Kitayama, N. Nukina, Modulation of monoamine transporter expression and function by repetitive transcranial magnetic stimulation, Biochemical and Biophysical Research Communications 327 (2005) 218–224.

[14] P. Chomczynski, N. Sacchi, Single-step method of RNA isolation by acid guanidinium thiocyanate-phenol-chloroform extraction, Analytical Biochemistry 162 (1987) 156–159.

[15] S.M. Tejani-Butt, D.J. Brunswick, A. Frazer, [^{3}H]nisoxetine: a new radioligand for norepinephrine uptake sites in brain, European Journal of Pharmacology 191 (1990) 239–243.

[16] G.H. Wang, K. Mitsui, S. Kotliarova, A. Yamashita, Y. Nagao, S. Tokuhiro, T. Iwatsubo, I. Kanazawa, N. Nukina, Caspase activation during apoptotic cell death induced by expanded polyglutamine in N2a cells, Neuroreport 10 (1999) 2435–2438.

[17] S. Kotliarova, N.R. Jana, N. Sakamoto, M. Kurosawa, H. Miyazaki, M. Nekooki, H. Doi, Y. Machida, H.K. Wong, T. Suzuki, C. Uchikawa, Y. Kotliarov, K. Uchida, Y. Nagao, U. Nagaoka, A. Tamaoka, K. Oyanagi, F. Oyama, N. Nukina, Decreased expression of hypothalamic neuropeptides in Huntington disease transgenic mice with expanded polyglutamine-EGFP fluorescent aggregates, Journal of Neurochemistry 93 (2005) 641–653.

[18] R.J. Lipshutz, S.P. Fodor, T.R. Gingeras, D.J. Lockhart, High density synthetic oligonucleotide arrays, Nature Genetics 21 (1999) 20–24.

Atlas of Genetics and Cytogenetics in Oncology and Haematology

Atlas of Genetics and Cytogenetics in Oncology and Haematology

SEARCH FOR Go Clear Advanced search

SPONSORS

Cerba European Lab

We need iconography of chromosomes

Atlas Journal : Table of Contents - Current and past Issues

1st International workshop on Cancer Genetic & Cytogenetic Diagnostics
March 20th to March 22nd, 2013
Radboud University Nijmegen Medical Centre, The Netherlands

- **ENTITIES: by THEME**

CANCER GENES A B C D E F G H I J K L M N O P Q R S T U V W X Y Z
LEUKAEMIAS
SOLID TUMOURS
CANCER PRONE DISEASES

- **ENTITIES: by CHROMOSOME**

X Y 1 2 3 4 5 6 7 8 9 10 11 12 13 14 15 16 17 18 19 20 21 22 Not Assigned

- **REVIEWS and CASE REPORTS**

DEEP INSIGHTS
CASE REPORTS (see also a list of Rare Translocations and Authors Instructions)

- **PORTAL**

DATABASES AND LINKS
JOURNALS

- **EDUCATIONAL ITEMS IN GENETICS**

EnglishFrenchGermanItalianSpanish

Recent papers in the Atlas

Genes partners

Tumour cell lines

The Atlas NEEDS MONEY : **Visit the site ARMGHM**,
the association in charge of the Atlas and **DONATE**!

Donate (in Euros) **Donate (in US Dollars)**

SCIENTIFIC SOCIETIES,
We need your editorial participation
and your financial support.
SPONSORING is also welcome.
Please, Contact us : Jean-Loup Huret, Editor

The Atlas needs

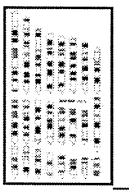

ISCN 2009

Cell Biology

Angiogenesis
Apoptosis
Cell cycle
Cell junction
Channel
Chromatin
Cytoskeleton
DNA repair
DNA replication-recombination

DPP4 (dipeptidyl-peptidase 4)

Identity

Other names **ADABP**
ADCP2
CD26
DPPIV
TP103

HGNC (Hugo) **DPP4**

LocusID (NCBI) **1803**

Location 2q24.2

Location_base_pair Starts at 162848755 and ends at 162931052 bp from pter (according to hg19-Feb_2009) [Mapping]

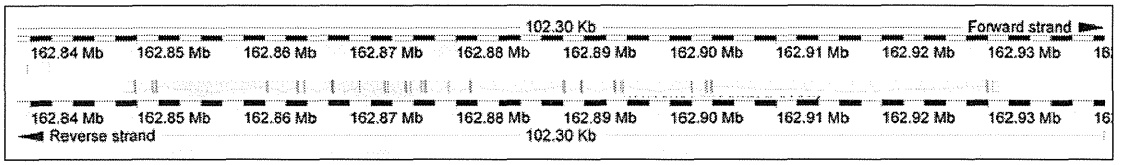

Location of DPP4 gene on chromosome 2q24.3. DPP4 spans 82,301 kbp of chromosome 2 from 162848751 to 162931052. The gene contains 26 exons (indicated in orange squares), ranging from 45 to 1,4 kb in length on the reverse strand. The Ser recognition site (G-W-S-Y-G) is split between exons 21 and 22.

DNA/RNA

Note

In 1979, a large molecular weight complex composed of adenosine deaminase (ADA) were reported to be found as an adenosine deaminase-binding protein (ADBP), also known as adenosine deaminase complexing protein-2 (ADCP2). In 1993, this adenosine deaminase-binding protein is determined to be identical to CD26, a T-cell activation molecule and a 110-kD glycoprotein that is present also on epithelial cells of various tissues including the liver, kidney, and intestine. The CD26 cDNA contains a 3465 bp open reading frame that encodes a 766 amino acid protein. The CD26 amino acid sequence has 85% amino acid identity with the mouse and rat CD26 genes and 37% amino acid identity with D. melanogaster. Two CD26 transcripts (4,2 and 2,8 kb) were found, both of which were expressed at high levels in the placenta and kidney and at moderate levels in the lung and liver. However, only the 4,2 kb mRNA was expressed at low levels in skeletal muscle, heart, brain, and pancreas.

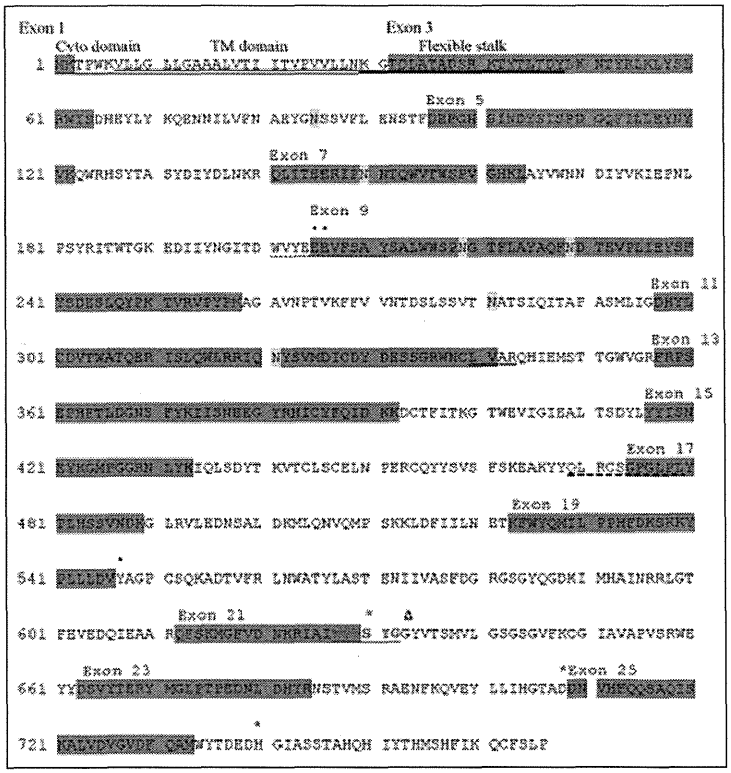

The schematic diagrams of the amino acids of DPP4. The cDNA of DPP4 is composed of 2301 base pairs, translated to 766 amino acid protein. CD26/DPP4 is a ubiquitous, membrane-bound enzyme that has roles in nutrition, metabolism, the immune and endocrine systems, bone marrow mobilization, cancer growth and cell adhesion. DDPIV catalyzes the hydrolysis of N-terminal dipeptides from polypeptides with proline or alanine in the penultimate position. Note: residues 1-6: cytoplasmic domain (MKTPWK); residues 7-29: transmembrane domain (VLLGLLGAAALVTI ITVPVVLLN);

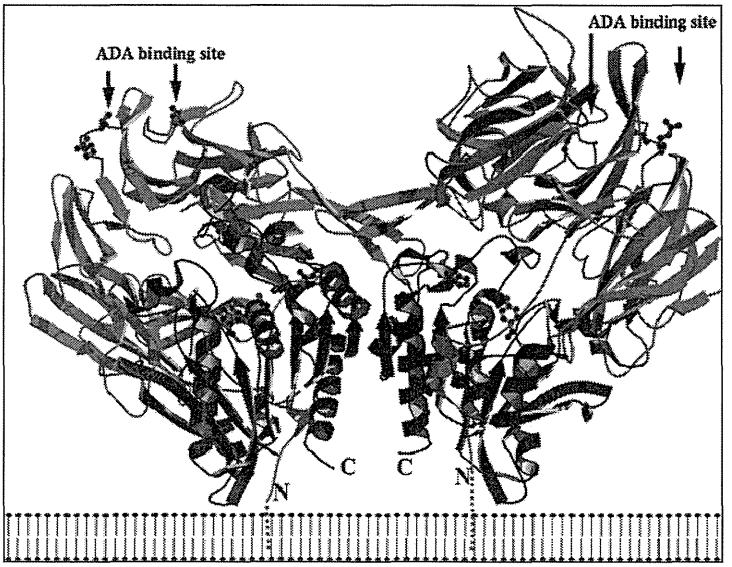

3-D structure of CD26/DPPIV. CD26/DPPIV forms a homodimer in the cell surface membrane. The residues 7-28 constitute the membrane spanning region. Each subunit consists of two domains, that is, an α/β-hydrolase domain and a β-propeller domain. The N-terminal β-propeller domain of CD26/DPPIV (residues 55-497) consists of 8 blades. β-strand 2 of blade 4 of the propeller extends into a small domain (residues 234-260) that includes an antiparallel two-stranded β-sheet. The function of this arm is to stabilize the dimeric structure. The catalytic site (Ser630-Asp708-His740) is located in a large cavity (also called a central tunnel), formed between the α/β-hydrolase domain and 8-bladed β-propeller domain, which contains the consensus sequence (DW(V/L)YEEE), that is common to S9b proteases. The central tunnel and α/β-hydrolase domains both participate in inhibitor binding. This figure is reproduced from Ralf Thoma et al., Structural Basis of Proline-Specific Exopeptidase Activity as Observed in Human Dipeptidyl Peptidase-IV, Structure 2003;8:947-959, with permission by Elsevier Limited.

Expression

CD26 is expressed in many tissues. Two CD26 transcripts (4,2 and 2,8 kb) are reported to be found, both of which were expressed at high levels in the placenta and kidney and at moderate levels in the lung and liver. The 4,2 kb transcript was expressed at low levels in skeletal muscle, heart, brain, and pancreas. Other organs expressing CD26 include: brain, endothelium, heart, intestine (colon adenocarcinoma, fetal colon expression disappears at birth), kidney, liver, lung, skeletal muscle, pancreas, and placenta. In the hematopoietic system CD26 is found on $CD4^+$ T memory cells, $CD8^+$ effector/memory T cells. It has been reported that 0-5% of freshly isolated $CD20^+$ B cells do express the CD26 antigen. Following stimulation with PMA (phorbol 12-Myristate 13-acetate) or Streptococcus aureus protein, the fraction of CD26-positive cells increased to 51%. Meanwhile, CD26 is not expressed or is found only at low levels on monocytes of healthy adult. Flow cytometric analysis of dendritic antigen-presenting cells (DC) generated from peripheral blood of normal donors in the presence of granulocyte/macrophage colony-stimulating factor and revealed intermediate levels of CD26 expression during a 2-week culture period. Only a small fraction of peripheral NK cells was found to express CD26.

Localisation

CD26 physically binds with ADA, an enzyme that plays a key role in the development and function of lymphoid tissues. ADA is essential for purine metabolism, with the loss of ADA leading to a clinical syndrome characterized by severe immunodeficiency. When the ADA inhibitor pentostatin was used in the treatment of recurrent T cell lymphomas, a significant reduction in circulating $CD26^+$ T cells was observed in treated patients. This finding is consistent with the fact that there is a physical association between CD26 and ADA on the surface of T lymphocytes. CD26 also interacts with CD45RO, a tyrosine phosphatase with a critical role in T cell signal transduction, at lipid rafts in peripheral blood T lymphocytes to modify cellular signaling events. A lipid raft is a cholesterol-rich microdomain in cell membrane, which plays an important role in signal transduction in T-cell regulation. CD26 interaction with lipid rafts in peripheral blood T-cells influences key cellular signaling events. Non-activated peripheral blood T-cells treated with the anti-CD26 mAb 1F7 increased CD26 recruitment to lipid rafts, resulting in increased tyrosine phosphorylation of c-Cbl, Zap70, Erk1/Erk2, $p56^{lck}$, and TCR-ζ. Interestingly, CD26 is associated with CD45 RA outside of lipid rafts in cord blood T cells, and the strong physical linkage of CD26 and CD45 RA may be responsible for the attenuation of cord blood T-cell activation signaling through CD26. In addition to cell surface expression, nuclear localization of CD26 has been reported in malignant mesothelioma and malignant T cell lines, and in human thyroid carcinomas, although little is known on the functional relevance of nuclear CD26. In addition to membrane bound CD26, soluble form of CD26 (sCD26) is also detected in the sera, urine, thoracic fluid and seminal fluid. sCD26 in the sera appears to be functioned as immune enhancing protein in antigen-presenting cell (APC).

Function

CD26 is a co-stimulatory molecule for T-cell signal transduction. While CD26 expression is enhanced following activation of resting T cells, $CD4^+CD26^{high}$ T cells respond maximally to recall antigens such as tetanus toxoid. Moreover, we have previously reproted that effector CD26-mediated costimulatory activity is exerted via its DPPIV enzymatic activity. In addition, $CD4^+$ T cells with in vitro transendothelial migratory capacity appear to express high CD26, indicating a role for CD26 in the migration of T cells, and patients with autoimmune diseases such as multiple sclerosis, Grave's disease, and rheumatoid arthritis (RA) have been found to have increased numbers of $CD4^+CD26^+$ T cells in inflamed tissues as well as in their peripheral blood, with enhancement of CD26 expression in these autoimmune diseases correlating with disease severity. Moreover, $CD26^{high}CD8^+$ T cells in humans belong to early effector memory T cells, and $CD26^{high}CD8^+$ T cells increase expression of granzyme B, TNF-α (tumor necrosis factor-α), IFN-γ and Fas ligand, and exert cytotoxic effect with CD26-mediated costimulation. CD26 binds to caveolin-1 on APC, and residues 201 to 211 of CD26 along with the serine catalytic site at residue 630, which constitute a pocket structure of CD26/DPPIV, contribute to binding to the caveolin-1 scaffolding domain. This region in CD26 contains a caveolin-binding domain (ΦXΦXXXXΦXXΦ; Φ and X depict aromatic residue and any amino acid, respectively), specifically **WVYEEEVFSAY** in CD26. These observations strongly support the notion that DPPIV enzyme activity is necessary to exert T-cell costimulatory activation via CD26 as demonstrated in our previous report using CD26 specific mAbs. The cytoplasmic tail of CD26 is responsible for T-cell costimulation induced by anti-CD3 plus caveolin-1. It has been identified that CARMA1 binds to the cytoplasmic tail of dimeric CD26, and that a PDZ domain in CARMA1 is necessary for binding to CD26. Following its phosphorylation, CARMA1 functions as a signaling intermediate downstream of PKCθ and upstream of IKK in the TCR signaling transduction pathway leading to NF-κB activation. Dimeric CD26, but not monomeric CD26, binds to CARMA1. The enzymatic pocket structure of the DPPIV catalytic site is necessary for binding of CD26 to caveolin-1, leading to the upregulation of CD86 expression on APC. Therefore, dimerization of CD26 is not only necessary for binding to caveolin-1, but also serves as a scaffolding structure for the cytoplasmic signaling molecule CARMA1. Overall, CD26 ligation by caveolin-1 on APC recruits CD26-interacting CARMA1 to lipid rafts, resulting in the formation of a CARMA1-Bcl10-MALT1-IKK complex,

CD40L (CD154) expression was mutually exclusive, with CD40L expressed on cells from more indolent diseases. CD26 expression in T-cell LBL/ALL was associated with a worse survival. The majority of patients with T-ALL express CD26 on the leukemic cell surface. There appears to be high CD26/DPPIV expression on T-lymphoblasts but only moderate DPPIV activity. Aldinucci et al. showed that CD26 is a marker of poor prognosis in T-cell cancer and is a predictive marker of poor response to 2'-deoxycoformycin, pentostatin. This effect was seen in vitro in CD26/ADA positive leukemia/lymphoma T-cell lines, primary $CD26^+$ T-cell cancers, and normal T-cells ($CD26^+$). Loss of CD26 appears to be characteristic of cutaneous T-cell lymphoma (CTCL) and has been suggested as a useful diagnostic marker.

Entity Sezary syndrome/mycosis fungoides

Note CD26 expression is absent or weak in other T-cell lymphomas such as mycosis fungoides (MF) and Sezary syndrome (SS). SS is a form of CTCL involving the blood and skin. Loss of CD26 appears to be characteristic of CTCL and has been suggested as a useful diagnostic marker. Chemokines and their receptors are involved in recruitment and homing of cancer cells to tissues of several tumors including non-Hodgkin's T-cell lymphomas. SS cells express CXCR4 and the skin generates its ligand, SDF-1, which may represent a target for the main destination of SS cells metastasizing to the skin. SDF-1 (CXCL12) is normally cleaved and inactivated by DPPIV mediated activity. An abnormal CD26-negative/dim T-cell population was found in a study of 66 of 69 samples from 28 SS/MF patients. These $CD26^{negative/dim\ T}$-cells were CD26 negative in 23 patients and CD26-weakly positive in 5 patients. Sokolowska-Wojdylo and colleagues found that absence of CD26 on CLA (cutaneous lymphocyte-associated antigen)$^+$ $CD4^+$ T-cells was 100% sensitive for SS in 7 patients. Also, the number of CD26-negative T-cells correlated with treatments in 2 patients for over 1 year in a longitudinal study. SS patients have decreased plasma DPPIV activity. Soluble CD26 reduces the SDF-1 mediated SS cell migratory response. Inhibition of DPPIV activity in the $CD26^+$ CTCL cell line Hut78 increases SDF-1-induced migration of SS cells. The SDF-1-CXCR4 interactions may mediate SS cell affinity for skin as a metastatic site via the regulatory activity of CD26.

Entity T-large granular lymphocyte lymphoproliferative disorder

Note CD26 expression is associated with a more aggressive clinical course in T-cell large granular lymphocyte leukemia (T-LGLL). T-LGLL patients with low expression of CD26 on T-LGLL cells had a more indolent course, while patients with high expression developed recurrent infections due to neutropenia. LGLL patients often have autoimmune diseases. CD26 expression on T-LGLL is associated with inhibition of myeloid progenitors, possibly explaining the neutropenia seen in these patients with higher levels of CD26 expression. CD26 on T-LGLL cells is unable to transmit antibody-mediated activation signals, unlike CD26 on normal T-cells, so CD26-related signaling may be aberrant in T-LGLL. In a recent report of a single institution long-term follow-up of 21 T-LGLL patients, 0 of 21 had CD26 expression.

Entity Breast cancer

Note Cheng et al. found that CD26 expressed on rat lung capillary endothelium mediated lung metastases of breast cancer cells by association with fibronectin. They studied the Fischer 344/CRJ rats, which have a CD26 Gly633Arg substitution, that leads to retention and degradation of the mutant protein in the endoplasmic reticulum, as a "protein knock-out" model to characterize the previously established role of CD26 in metastasis. They found that lung metastases from the highly metastatic MTF7 rat breast cancer cell line were reduced by only 33% relative to normal Fischer 344 rats. Detailed immunohistochemical experiments revealed low levels of mutant enzymatically inactive CD26 on lung endothelial cells. When the mutant CD26 was purified, it had identical adhesion qualities for breast cancer cells as wild type DPPIV. The CD26/fibronectin-mediated adhesion and metastasis are effectively competed by soluble CD26, anti-CD26 mAb 6A3, and anti-fibronectin antiserum. Furthermore, peptides containing the fibronectin CD26-binding domain blocked the CD26-fibronectin interaction and significantly decreased pulmonary metastasis of breast cancer and melanoma cell lines. The utilization of fibronectin by cancer cells and fibronectin self-association in the blood suggests that CD26/fibronectin binding may be a mechanism for lung metastasis. CD26 is associated with increased topoisomerase IIa levels and tumor sensitivity to the topoisomerase II inhibitors, such as doxorubicin and etoposide. Recent studies suggest that topoisomerase IIα level is a prognostic factor in breast cancer that is independent of stage, Her-2/neu status, and histological grading. Furthermore, anthracycline treatment did not reverse the negative prognostic effect of topoisomerase IIα expression. Others have found, in retrospective studies that topoisomerase IIα overexpression confers a higher probability of response to doxorubicin. Topoisomerase IIα is currently being evaluated prospectively as a breast cancer predictive marker. The role of CD26 in breast cancer and the interaction of CD26 with topoisomerase IIα is an area for future research.

Entity Colon cancer

Note CD26 is found on the cell surface and its level correlates with disease status and tumor biology for certain cancers. In colorectal cancer, soluble CD26 (sCD26) in the sera was not related to colon cancer grade, stage, or location. The DPPIV inhibitor PT-100 (Val-boro-Pro) improved the activity of trastuzumab in human $Her2^+$ colon cancer in xenograft models. However, the anti-cancer activity of PT-100 was not changed in $CD26^{-/-}$ mice, suggesting non-CD26 mediated activity. Cordero et al. found that the sCD26 concentration is diminished in serum of colorectal cancer patients compared to healthy donors, suggesting the potential utility of a sCD26 immunochemical detection test for early diagnosis. Pang et al. have identified a subpopulation of $CD26^+$ cells uniformly present in both the primary and metastatic tumors in colorectal cancer patients with liver metastasis. Furthermore, in patients without distant metastasis at the time of presentation, the presence of $CD26^+$ cells in their primary tumors predicted distant metastasis on follow-up.

Entity Lung cancer

Note CD26 is expressed in lung adenocarcinoma but not other subtypes of lung cancer. CD26 expression and DPPIV activity are present in normal bronchial and alveolar epithelium, but non-adenocarcinoma lung cancers lose CD26 expression. CD26 downregulation may contribute to the loss of growth control in non-small cell lung carcinoma (NSCLC) cells. NSCLC cells transfected with CD26 develop morphologic changes, altered contact inhibition, and reduced ability for anchorage-independent growth. An increased percentage of cells in G0-G1 was noted in CD26 expressing cells, indicating CD26 may promote cell cycle arrest. Amatya and colleagues assessed the diagnostic utility of caveolin-1 (Cav-1), a ligand for CD26, which is expressed in endothelial cells, alveolar type I pneumocytes and mesothelial cells, as a novel positive marker of mesothelioma. Immunohistochemical study of 80 cases of epithelioid mesothelioma and 80 cases of lung adenocarcinoma was performed for the analysis of the expression of Cav-1 and other markers. Cav-1 expression with a membranous and/or cytoplasmic pattern was found in all of the epithelioid mesothelioma. Of these, 42 cases (52,5%) showed Cav-1 expression in >50% of tumour cells, 34 cases (42,5%) in 6-50% of tumour cells, and four cases (5,0%) in <5% of tumour cells. In contrast, only six cases (7,5%) of lung adenocarcinoma showed focal Cav-1 expression in the cytoplasm of the tumour cells. They concluded that Cav-1 is a novel immunohistochemical marker for the differentiation of epithelioid mesothelioma from lung adenocarcinoma.

transplanted SCID mice. In addtion, it has been shown that cells from certain CD26-positive mesothelioma cell lines appeared to include the cancer stem cell characteristics for malignant mesothelioma in addition to CD24 and CD9-positive cells. Furthermore, Morimoto et al. showed that the CD26 molecule is expressed on the cell membrane of the epithelial and biphasic, but not the sarcomatoid, type of mesothelioma. Importantly, treatment outcome prediction study showed that CD26 membrane expression on MPM was closely correlated with disease responsiveness to chemotherapy. Meanwhile, in vitro studies showed that mesothelioma cells expressing high level of CD26 displayed high proliferative activity, and microarray analysis of CD26 knockdown and CD26-transfected mesothelioma cells showed that CD26 expression was closely linked to expression of genes contributing to cell proliferation, cell cycle regulation, drug-induced apoptotic action, and chemotherapy resistance. These data therefore strongly suggest that the CD26 molecule is a good therapeutic target for MPM and a clinically significant biomarker for the prediction of response to chemotherapy for MPM.

Entity Gastric gastrointestinal stromal tumors

Note In an immunohistochemical analysis of 152 patients with gastric gastrointestinal stromal tumors (GIST), CD26 expression was found to be associated with a poorer overall survival.

Entity Rheumatoid arthritis

Note Rheumatoid arthritis (RA) is a chronic, inflammatory autoimmune disease and is characterized by progressive invasion of synovial fibroblasts into the articular cartilage and erosion of the undelying bone, followed by joint destruction. In antigen-induced arthritis mouse model, $DPPIV^{-/-}$ mice showed more severe arthritis, and enzymatic activity levels of DPPIV in the plasma were significantly decreased in RA patients. Morever, other investigators reported that inhibition of DPPIV and FAP increases cartilage invasion by RA synovial fibroblasts. However, CD26/DPPIV regulates biologic processes that are unrelated to its peptidase activity, e.g., cellular adhesion, cell differentiation, and activation via downstream signaling cascade. $CD26^{+}$ T cells induce the inflammation and tissue destruction characteristic of RA by migrating to and being active in the rheumatoid synovium. Cordero et al. studied IL-12, IL-15, soluble CD26, and ADA serum levels from 35 patients with active and inactive RA as well as those of controls. Patients' sera had higher IL-12 and IL-15 levels, and the level of soluble CD26 was inversely correlated with the number of swollen joints. These findings suggest that these cytokines and CD26 are associated with the inflammation and immune activity in RA. Mavropoulos et al. found that anti-TNF-α therapy increases DPPIV activity and decreases autoantibodies to the chaperone protein Bip (GRP78) and phosphoglucose isomerase in 15 patients with RA. DPPIV inhibitors inhibit a rat model of rheumatoid arthritis in a dose-dependent manner. Ohnuma et al. described $CD26^{+}$ T cells infiltrating the rheumatoid synovium using immunohistochemical studies. They found high expression of caveolin-1 in the rheumatoid synovium vasculature and synoviocytes. These data suggest that the CD26-caveolin-1 upregulation of CD86 on activated monocytes leads to antigen-specific T-cell activation in rheumatoid arthritis. DPPIV inhibitors may be useful for suppressing the immune system in rheumatoid arthritis and other autoimmune diseases.

Entity Inflammatory bowel diseases

Note Crohn's disease and ulcerative colitis are categorized as inflammatory bowel disease (IBD), being characterized by chronic remittent or progressive inflammatory conditions that may affect the entire gastrointestinal tract and the colonic mucosa, respectively, and are associated with an increased risk for colon cancer. Sera from IBD patients contain lower levels of circulating DPPIV activity, while membrane expression of CD26/DPPIV on T cells isolated from IBD patients is higher than healthy controls. These clinical observations indicate that CD26/DPPIV might play a significant role in perpetuating the inflammatory response associated with IBD.

Entity Systemic lupus erythematosus

Note Serum levels of soluble CD26 and its specific DPPIV activity were significantly decreased in patients with systemic lupus erythematosus (SLE), and were inversely correlated with SLE disease activity index score, but not with clinical variables or clinical subsets of SLE. More recently, Lam et al. reported that CD26 expression on invariant natural killer cells of SLE patients is decreased significantly than that of healthy controls.

External links

	Nomenclature
HGNC (Hugo)	DPP4 3009
Entrez_Gene (NCBI)	DPP4 1803 dipeptidyl-peptidase 4
	Cards
Atlas	**DPP4ID40360ch2q24**
GeneCards (Weizmann)	DPP4
Ensembl (Hinxton)	ENSG00000197635 [Gene_View] chr2:162848755-162931052 [Contig_View] DPP4 [Vega]
AceView (NCBI)	DPP4
Genatlas (Paris)	DPP4
SOURCE (Stanford)	NM_001935
	Genomic and cartography
GoldenPath (UCSC)	DPP4 - 2q24.2 chr2:162848755-162931052 - 2q23-qter [Description] (hg19-Feb_2009)
Ensembl	DPP4 - 2q23-qter [CytoView]
Mapping of homologs : NCBI	DPP4 [Mapview]
OMIM	102720
	Gene and transcription
Genbank (Entrez)	AB451339 AB451488 AK314798 AY429531 AY429532
RefSeq transcript (SRS)	NM_001935
RefSeq transcript (Entrez)	NM_001935
RefSeq genomic (SRS)	AC_000134 NC_000002 NC_018913 NT_005403 NW_001838860 NW_004078008

SNP Single Nucleotide Polymorphism (NCBI)	
SNP (GeneSNP Utah)	DPP4
SNP : HGBase	DPP4
Genetic variants : HAPMAP	DPP4
Somatic Mutations in Cancer : COSMIC	DPP4
CONAN: Copy Number Analysis	DPP4
Mutations and Diseases : HGMD	DPP4
OMIM	102720
GENETests	102720
Disease Genetic Association	DPP4
Huge Navigator	DPP4 [HugePedia] DPP4 [HugeCancerGEM]
Genomic Variants	DPP4 DPP4 [DGVbeta]
snp3D : Map Gene to Disease	1803
	General knowledge
Homologs : HomoloGene	DPP4
Homology/Alignments : Family Browser (UCSC)	DPP4
Phylogenetic Trees/Animal Genes : TreeFam	DPP4
Catalytic activity : Enzyme	3.4.14.5 [Enzyme-Expasy] 3.4.14.5 [Enzyme-SRS] 3.4.14.5 [IntEnz-EBI] 3.4.14.5 [BRENDA] 3.4.14.5 [KEGG]
Chemical/Protein Interactions : CTD	1803
Chemical/Pharm GKB Gene	PA27467
Clinical trial	DPP4
Cancer Resource (Charite)	ENSG00000197635
Ontology : AmiGO	response to hypoxia protease binding regulation of T cell mediated immunity aminopeptidase activity serine-type endopeptidase activity receptor binding protein binding collagen binding endoplasmic reticulum Golgi apparatus plasma membrane proteolysis cell adhesion serine-type peptidase activity dipeptidyl-peptidase activity positive regulation of cell proliferation cell surface negative regulation of extracellular matrix disassembly integral to membrane apical plasma membrane lamellipodium endocytic vesicle lamellipodium membrane T cell costimulation regulation of cell-cell adhesion mediated by integrin T cell activation peptide binding protein homodimerization activity endothelial cell migration membrane raft intercellular canaliculus establishment of localization extracellular vesicular exosome invadopodium membrane
Ontology : EGO-EBI	response to hypoxia protease binding regulation of T cell mediated immunity aminopeptidase activity serine-type endopeptidase activity receptor binding protein binding collagen binding endoplasmic reticulum Golgi apparatus plasma membrane proteolysis cell adhesion serine-type peptidase activity dipeptidyl-peptidase activity positive regulation of cell proliferation cell surface negative regulation of extracellular matrix disassembly integral to membrane apical plasma membrane lamellipodium endocytic vesicle lamellipodium membrane T cell costimulation regulation of cell-cell adhesion mediated by integrin T cell activation peptide binding protein homodimerization activity endothelial cell migration membrane raft intercellular canaliculus establishment of localization extracellular vesicular exosome invadopodium membrane
	Other databases
	Probes
	Litterature
PubMed	**239 Pubmed reference(s) in Entrez**
PubGene	DPP4
iHOP	DPP4

Bibliography

Cell surface antigens of human melanocytes and melanoma. Expression of adenosine deaminase binding protein is extinguished with melanocyte transformation.
Houghton AN, Albino AP, Cordon-Cardo C, Davis LJ, Eisinger M.
J Exp Med. 1988 Jan 1;167(1):197-212.
PMID 2891780

Dipeptidyl aminopeptidase IV staining of cytologic preparations to distinguish benign from malignant thyroid diseases.
Aratake Y, Kotani T, Tamura K, Araki Y, Kuribayashi T, Konoe K, Ohtaki S.
Am J Clin Pathol. 1991 Sep;96(3):306-10.
PMID 1715126

Expression of dipeptidyl aminopeptidase IV activity in thyroid carcinoma.
Kotani T, Aratake Y, Ogata Y, Umeki K, Araki Y, Hirai K, Kuma K, Ohtaki S.
Cancer Lett. 1991 May 24;57(3):203-8.
PMID 1674445

Diagnostic usefulness of dipeptidyl aminopeptidase IV monoclonal antibody in paraffin-embedded thyroid follicular tumours.

Dipeptidyl peptidase IV (DP IV, CD26) in patients with inflammatory bowel disease.
Hildebrandt M, Rose M, Ruter J, Salama A, Monnikes H, Klapp BF.
Scand J Gastroenterol. 2001 Oct;36(10):1067-72.
PMID 11589380

In vitro and in vivo antitumor effect of the anti-CD26 monoclonal antibody 1F7 on human CD30+ anaplastic large cell T-cell lymphoma Karpas 299.
Ho L, Aytac U, Stephens LC, Ohnuma K, Mills GB, McKee KS, Neumann C, LaPushin R, Cabanillas F, Abbruzzese JL, Morimoto C, Dang NH.
Clin Cancer Res. 2001 Jul;7(7):2031-40.
PMID 11448921

CD26-mediated signaling for T cell activation occurs in lipid rafts through its association with CD45RO.
Ishii T, Ohnuma K, Murakami A, Takasawa N, Kobayashi S, Dang NH, Schlossman SF, Morimoto C.
Proc Natl Acad Sci U S A. 2001 Oct 9;98(21):12138-43. Epub 2001 Oct 2.
PMID 11593028

Absence of CD26 expression is a useful marker for diagnosis of T-cell lymphoma in peripheral blood.
Jones D, Dang NH, Duvic M, Washington LT, Huh YO.
Am J Clin Pathol. 2001 Jun;115(6):885-92.
PMID 11392886

Soluble CD26/dipeptidyl peptidase IV induces T cell proliferation through CD86 up-regulation on APCs.
Ohnuma K, Munakata Y, Ishii T, Iwata S, Kobayashi S, Hosono O, Kawasaki H, Dang NH, Morimoto C.
J Immunol. 2001 Dec 15;167(12):6745-55.
PMID 11739489

Prolonged survival and decreased invasive activity attributable to dipeptidyl peptidase IV overexpression in ovarian carcinoma.
Kajiyama H, Kikkawa F, Suzuki T, Shibata K, Ino K, Mizutani S.
Cancer Res. 2002 May 15;62(10):2753-7.
PMID 12019149

Reduction of serum soluble CD26/dipeptidyl peptidase IV enzyme activity and its correlation with disease activity in systemic lupus erythematosus.
Kobayashi H, Hosono O, Mimori T, Kawasaki H, Dang NH, Tanaka H, Morimoto C.
J Rheumatol. 2002 Sep;29(9):1858-66.
PMID 12233879

G1/S cell cycle arrest provoked in human T cells by antibody to CD26.
Ohnuma K, Ishii T, Iwata S, Hosono O, Kawasaki H, Uchiyama M, Tanaka H, Yamochi T, Dang NH, Morimoto C.
Immunology. 2002 Nov;107(3):325-33.
PMID 12423308

Effect of CD26/dipeptidyl peptidase IV on Jurkat sensitivity to G2/M arrest induced by topoisomerase II inhibitors.
Aytac U, Sato K, Yamochi T, Yamochi T, Ohnuma K, Mills GB, Morimoto C, Dang NH.
Br J Cancer. 2003 Feb 10;88(3):455-62.
PMID 12569391

A novel consensus motif in fibronectin mediates dipeptidyl peptidase IV adhesion and metastasis.
Cheng HC, Abdel-Ghany M, Pauli BU.
J Biol Chem. 2003 Jul 4;278(27):24600-7. Epub 2003 Apr 25.
PMID 12716896

T-large granular lymphocyte lymphoproliferative disorder: expression of CD26 as a marker of clinically aggressive disease and characterization of marrow inhibition.
Dang NH, Aytac U, Sato K, O'Brien S, Melenhorst J, Morimoto C, Barrett AJ, Molldrem JJ.
Br J Haematol. 2003 Jun;121(6):857-65.
PMID 12786796

Dipeptidyl peptidase IV overexpression induces up-regulation of E-cadherin and tissue inhibitors of matrix metalloproteinases, resulting in decreased invasive potential in ovarian carcinoma cells.
Kajiyama H, Kikkawa F, Khin E, Shibata K, Ino K, Mizutani S.
Cancer Res. 2003 May 1;63(9):2278-83.
PMID 12727850

Immunohistochemical detection of dipeptidyl peptidase IV (CD 26) in thyroid neoplasia using biotinylated tyramine amplification.
Kholova I, Ludvikova M, Ryska A, Hanzelkova Z, Cap J, Pecen L, Topolcan O.
Neoplasma. 2003;50(3):159-64.
PMID 12937847

CD26/dipeptidyl peptidase IV enhances expression of topoisomerase II alpha and sensitivity to apoptosis induced by topoisomerase II inhibitors.
Sato K, Aytac U, Yamochi T, Yamochi T, Ohnuma K, McKee KS, Morimoto C, Dang NH.
Br J Cancer. 2003 Oct 6;89(7):1366-74.
PMID 14520473

Structural basis of proline-specific exopeptidase activity as observed in human dipeptidyl peptidase-IV.
Thoma R, Loffler B, Stihle M, Huber W, Ruf A, Hennig M.
Structure. 2003 Aug;11(8):947-59.
PMID 12906826

CD26/dipeptidyl peptidase IV as a novel therapeutic target for cancer and immune disorders.
Thompson MA, Ohnuma K, Abe M, Morimoto C, Dang NH.
Mini Rev Med Chem. 2007 Mar;7(3):253-73. (REVIEW)
PMID 17346218

The role of CD26/dipeptidyl peptidase IV in cancer.
Havre PA, Abe M, Urasaki Y, Ohnuma K, Morimoto C, Dang NH.
Front Biosci. 2008 Jan 1;13:1634-45. (REVIEW)
PMID 17981655

Revisiting an old acquaintance: CD26 and its molecular mechanisms in T cell function.
Ohnuma K, Dang NH, Morimoto C.
Trends Immunol. 2008 Jun;29(6):295-301. doi: 10.1016/j.it.2008.02.010. Epub 2008 May 2. (REVIEW)
PMID 18456553

Role of CD26/dipeptidyl peptidase IV in human T cell activation and function.
Ohnuma K, Takahashi N, Yamochi T, Hosono O, Dang NH, Morimoto C.
Front Biosci. 2008 Jan 1;13:2299-310. (REVIEW)
PMID 17981712

Caveolin-1 is a novel immunohistochemical marker to differentiate epithelioid mesothelioma from lung adenocarcinoma.
Amatya VJ, Takeshima Y, Kohno H, Kushitani K, Yamada T, Morimoto C, Inai K.
Histopathology. 2009 Jul;55(1):10-9. doi: 10.1111/j.1365-2559.2009.03322.x.
PMID 19614762

CD26 expression on T cell lines increases SDF-1-alpha-mediated invasion.
Havre PA, Abe M, Urasaki Y, Ohnuma K, Morimoto C, Dang NH.
Br J Cancer. 2009 Sep 15;101(6):983-91. doi: 10.1038/sj.bjc.6605236. Epub 2009 Aug 4.
PMID 19654580

Blockade of CD26-mediated T cell costimulation with soluble caveolin-1-Ig fusion protein induces anergy in CD4+T cells.
Ohnuma K, Uchiyama M, Hatano R, Takasawa W, Endo Y, Dang NH, Morimoto C.
Biochem Biophys Res Commun. 2009 Aug 21;386(2):327-32. doi: 10.1016/j.bbrc.2009.06.027. Epub 2009 Jun 10.
PMID 19523449

Decreased expression of T lymphocyte co-stimulatory molecule CD26 on invariant natural killer T cells in systemic lupus erythematosus.
Wong PT, Wong CK, Tam LS, Li EK, Chen DP, Lam CW.
Immunol Invest. 2009;38(5):350-64.
PMID 19811413

Localization of CD26/DPPIV in nucleus and its nuclear translocation enhanced by anti-CD26 monoclonal antibody with anti-tumor effect.
Yamada K, Hayashi M, Du W, Ohnuma K, Sakamoto M, Morimoto C, Yamada T.
Cancer Cell Int. 2009 Jun 26;9:17. doi: 10.1186/1475-2867-9-17.
PMID 19555512

A subpopulation of CD26+ cancer stem cells with metastatic capacity in human colorectal cancer.
Pang R, Law WL, Chu AC, Poon JT, Lam CS, Chow AK, Ng L, Cheung LW, Lan XR, Lan HY, Tan VP, Yau TC, Poon RT, Wong BC.
Cell Stem Cell. 2010 Jun 4;6(6):603-15. doi: 10.1016/j.stem.2010.04.001.
PMID 20569697

Inhibition of dipeptidyl peptidase 4 regulates microvascular endothelial growth induced by inflammatory cytokines.
Takasawa W, Ohnuma K, Hatano R, Endo Y, Dang NH, Morimoto C.
Biochem Biophys Res Commun. 2010 Oct 8;401(1):7-12. doi: 10.1016/j.bbrc.2010.08.112. Epub 2010 Sep 7.
PMID 20828536

Mechanisms of confluence-dependent expression of CD26 in colon cancer cell lines.
Abe M, Havre PA, Urasaki Y, Ohnuma K, Morimoto C, Dang LH, Dang NH.
BMC Cancer. 2011 Feb 1;11:51. doi: 10.1186/1471-2407-11-51.
PMID 21284881

Dipeptidyl peptidase in autoimmune pathophysiology.
Ohnuma K, Hosono O, Dang NH, Morimoto C.
Adv Clin Chem. 2011;53:51-84. (REVIEW)
PMID 21404914

CD26 overexpression is associated with prolonged survival and enhanced chemosensitivity in malignant pleural mesothelioma.
Aoe K, Amatya VJ, Fujimoto N, Ohnuma K, Hosono O, Hiraki A, Fujii M, Yamada T, Dang NH, Takeshima Y, Inai K, Kishimoto T, Morimoto C.
Clin Cancer Res. 2012 Mar 1;18(5):1447-56. doi: 10.1158/1078-0432.CCR-11-1990. Epub 2012 Jan 18.
PMID 22261805

CD26-mediated co-stimulation in human CD8(+) T cells provokes effector function via pro-inflammatory cytokine production.
Hatano R, Ohnuma K, Yamamoto J, Dang NH, Morimoto C.
Immunology. 2013 Feb;138(2):165-72. doi: 10.1111/imm.12028.
PMID 23113658

REVIEW articles *automatic* search in PubMed
Last year publications *automatic* search in PubMed

Search in all

EBI NCBI